

# Invariant manifolds and the parameterization method in coupled energy harvesting piezoelectric oscillators\*

Albert Granados<sup>†</sup>

## Abstract

Energy harvesting systems based on oscillators aim to capture energy from mechanical oscillations and convert it into electrical energy. Widely extended are those based on piezoelectric materials, whose dynamics are Hamiltonian submitted to different sources of dissipation: damping and coupling. These dissipations bring the system to low energy regimes, which is not desired in long term as it diminishes the absorbed energy. To avoid or to minimize such situations, we propose that the coupling of two oscillators could benefit from theory of Arnold diffusion. Such phenomenon studies  $O(1)$  energy variations in Hamiltonian systems and hence could be very useful in energy harvesting applications. This article is a first step towards this goal. We consider two piezoelectric beams submitted to a small forcing and coupled through an electric circuit. By considering the coupling, damping and forcing as perturbations, we prove that the unperturbed system possesses a 4-dimensional Normally Hyperbolic Invariant Manifold with 5 and 4-dimensional stable and unstable manifolds, respectively. These are locally unique after the perturbation. By means of the parameterization method, we numerically compute parameterizations of the perturbed manifold, its stable and unstable manifolds and study its inner dynamics. We show evidence of homoclinic connections when the perturbation is switched on.

**Keywords:** damped oscillators, parameterization method, normally hyperbolic invariant manifolds, homoclinic connections.

---

\*This work has been partially supported by MINECO MTM2015-65715-P Spanish grant and Marie Curie FP7 COFUND Ørsted fellowship. We acknowledge the use of the UPC Dynamical Systems group's cluster for research computing (<https://dynamicalsystems.upc.edu/en/computing/>)

<sup>†</sup>algr@dtu.dk, Department of Applied Mathematics and Computer Science, Technical University of Denmark, Building 303B, 2800 Kgs. Lyngby, Denmark.

# Contents

<b>1</b>	<b>Introduction</b>	<b>2</b>
<b>2</b>	<b>Invariant objects</b>	<b>6</b>
2.1	Unperturbed system . . . . .	6
2.2	Persistence of manifolds . . . . .	15
<b>3</b>	<b>Numerical framework for the parameterization method</b>	<b>16</b>
3.1	A Newton-like method . . . . .	18
3.1.1	First step: correction of the manifold and the inner dynamics . . . . .	19
3.1.2	Second step: normal bundle correction . . . . .	20
3.2	Computation of bundles, maps and frames for the unper- turbed case . . . . .	22
<b>4</b>	<b>Numerical results</b>	<b>25</b>
4.1	Conservative case . . . . .	26
4.2	Dissipative case . . . . .	32
4.2.1	Weak damping . . . . .	32
4.2.2	Weak dissipative coupling . . . . .	36
<b>5</b>	<b>Conclusions</b>	<b>41</b>

## 1 Introduction

Energy harvesting systems consists of devices able to absorb energy from the environment and, typically, electrically power a load or accumulate electrical energy in accumulators (super capacitors or batteries) for later use. One of the most extended approaches is by means of piezoelectric materials, which, under a mechanical strain, generate an electric charge. Such materials are however mostly observed working in the inverse way in, for example, most cell phones: they generate a vibration from a varying voltage source.

Most energy harvesting systems based on piezoelectric materials aim to absorb energy from machine vibrations, pedestrian walks or wind turbulences, and can power loads ranging from tiny sensors from small vibrations to small communities through networks of large piezoelectric “towers” submitted to wind turbulences. One of the most extended configurations consists of a piezoelectric beam or cantilever. Due to the elastic nature of the piezoelectric materials, they behave like damped oscillators which, in absence of a

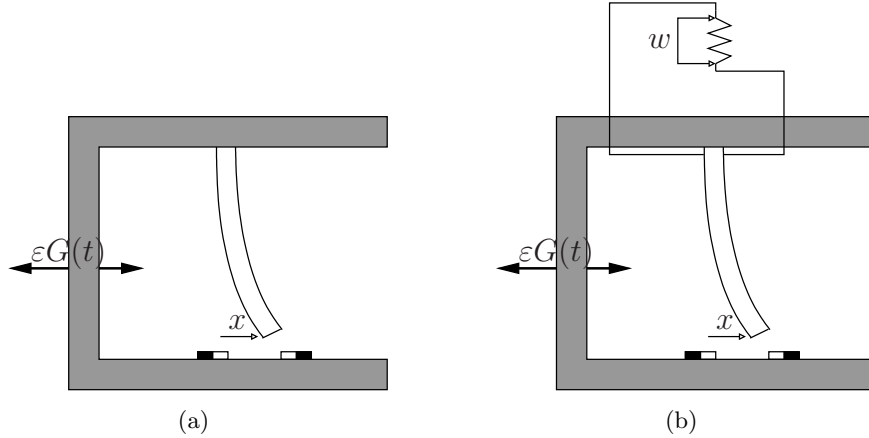


Figure 1: Generic elastic beam (a) and piezoelectric beam (b) subject to the influence of two magnets and a small periodic forcing.

strong enough external forcing, tend to oscillate with small amplitude close to the resting position. In order to benefit higher energy oscillations, a typical approach consists of locating two magnets in inverse position as in Figure 1(b). If the magnets are strong enough with respect to the damping of the beam, in the absence of an external forcing, the resting vertical position (previously an attracting focus) becomes a saddle equilibrium and two new attracting foci appear pointing to each of the magnets.

The equations of motions for a generic (not necessarily piezoelectric) damped and forced beam with magnets as the one shown in Figure 1(a) were first derived in [23], which were shown to be a Duffing equation:

$$\ddot{x} + 2\zeta\dot{x} - \frac{1}{2}x(1 - x^2) = \varepsilon G(t),$$

where  $x$  is the dimensionless displacement of the lower end,  $\zeta$  is the damping coefficient and  $\varepsilon G(t)$  a small periodic forcing. When a piezoelectric beam is connected to a load in the upper end (as in Figure 1(b)), the load receives a certain power, a voltage  $w$ , whose time-derivative is proportional to the speed of lower displacement. From the point of view of the load, the piezoelectric beam acts as a capacitor. Hence, the voltage  $w$  follows the discharge law of a capacitor:

$$\dot{w} = -\lambda w - \kappa\dot{x},$$

where  $\lambda$  is a time constant associated with the capacitance of the piezoelectric beam and the resistance of the load, and  $\kappa > 0$  is the electrical

piezoelectric constant. However, in such a configuration, a mechanical auto-coupling effect occurs: the beam sees its own generated voltage  $w$  and the piezoelectric properties of the beam generates a strain opposite to the currently applied one. This not only has a dissipative effect, as it slows down the beam, but also increases the dimension of the system by one (see [9]), which becomes:

$$\begin{aligned}\ddot{x} + 2\zeta\dot{x} - \frac{1}{2}x(1 - x^2) - \chi w &= \varepsilon G(t) \\ \dot{w} &= -\lambda w - \kappa\dot{x},\end{aligned}$$

where  $\chi > 0$  is the mechanical piezoelectric constant.

The length of a piezoelectric beams or cantilevers plays a crucial role in the efficiency of the energy harvesting system, as it determines the frequency of the external forcing,  $\varepsilon G(t)$ , for which the device is “optimal”. Therefore, such devices need to be designed to resonate at a particular frequency. A big effort has been done from the design point of view to broaden this bandwidth. A common approach, introduced in [19], is to consider coupled oscillators of different lengths such that the device exhibits different voltage peaks at different frequencies. Other approaches consider different structural configurations ([11]) to achieve a similar improvement, or study the number of piezoelectric layers connected in different series-parallel configurations ([10]). However, mathematical studies of those models seem relegated to numerical simulations and bifurcation analysis [14, 25, 26]. As it was unveiled in [23], there exist very interesting dynamical phenomena already in the most simple case of a single beam under a periodic forcing, such as homoclinic tangles and horseshoes; also, in the absence of damping, KAM theory holds to show the existence of invariant curves. These, in the absence of damping, are boundaries in the state space and hence act as energy bounds. Therefore, assuming an external forcing of  $O(\varepsilon)$ , the amplitude of the oscillations of the beam cannot grow beyond this order hence restricting the amount of energy that can be absorbed from the source.

Even more interesting from the dynamical point of view is the higher dimensional case when considering two or more coupled damped oscillators. In this case, in the absence of damping, the dimension of KAM tori is not large enough to act as energy bounds and one may observe *Arnold diffusion*: existence of trajectories exhibiting  $O(1)$  changes in their “energy” when the device is driven by an arbitrarily small periodic forcing. Introduced in the celebrated paper of Arnold [1], researchers have recently achieved important rigorous results to prove the existence of such trajectories in general Hamiltonian systems [2, 22, 15]. The most paradigmatic applications of Arnold

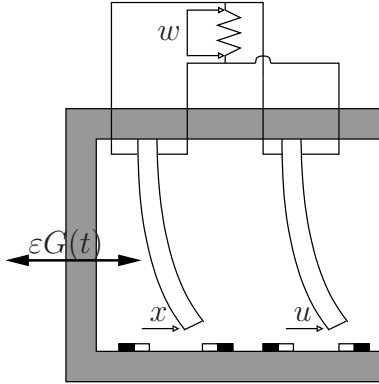


Figure 2: Energy harvester based on two piezoelectric beams.

diffusion are associated with classical problems in celestial mechanics such as the *restricted three-body problem* and the Kirkwood gaps in the asteroids belt of the solar system [12], although it has also been proven in physical examples such as ABC magnetic fields [21].

The phenomenon of Arnold diffusion may be also relevant from a more applied point of view, for example related instabilities in mechanical structures can be very destructive, although it is desirable in energy harvesting systems and might help to improve their performance. Unfortunately, in real applications, one frequently finds obstacles such as dissipation or lack of regularity in order to apply the existent theory. For the latter, there has been already theoretical contributions with applications to impacting mechanics [16].

In this work we present a first step on the study of Arnold diffusion in energy harvesting systems based on damped oscillators. In particular, we focus on a system based on the coupling of two piezoelectric beams as in Figure 2 and we perform a numerical study of the invariant objects and their connections by means of the parameterization method. These play a crucial role in the known mechanisms for Arnold diffusion, which combine dynamics close to Normally Hyperbolic Invariant Manifolds (NHIM's) (*inner dynamics*) and *heteroclinic/homoclinic excursions* along the intersection of their stable and unstable manifolds. The study of the latter excursions was greatly facilitated after the introduction of the *scattering map* [7, 8]. In this article we have a less ambitious goal and we perform a first step in this direction: we perform a theoretical study of the existence and persistence of a NHIM, its numerical computation as well as its inner dynamics and its stable and unstable manifolds by means of the so-called *parameteriza-*

*tion method* [5, 18]. A detailed study of homoclinic intersections and the scattering map is left for a future work. The main difficulty relies on the dimension of the system, which is 6-dimensional and the presence of dissipation in both the oscillators (through damping) and the coupling (inverse piezoelectric effect).

This work is organized as follows. In Section 2 we introduce the system in a perturbation setting: forcing and dissipation are included only in  $O(\varepsilon)$  terms. We analyze its invariant objects for the unperturbed case and their persistence after introducing the perturbation. In Section 3 we present the theoretical setting necessary to apply a Newton-like method introduced in [18] based on the parameterization method. In Section 4 we present the obtained numerical results, studying the inner dynamics for different configurations regarding the two type of dissipations (damping and piezoelectric coupling). Finally, we present our conclusions in Section 5.

## 2 Invariant objects

### 2.1 Unperturbed system

Let  $x$  and  $u$  be the displacements of the both piezoelectric beams, and let  $y = \dot{x}$  and  $v = \dot{u}$ . Calling  $w$  the (dimensionless) voltage on the resistor and adding time as a variable, from [20] we have that the equations of the model are

$$\begin{aligned}
 \dot{x} &= y \\
 \dot{y} &= -2\zeta y + \frac{1}{2}x(1-x^2) + \chi w + \varepsilon G(s) \\
 \dot{u} &= v \\
 \dot{v} &= -2\zeta v + \frac{1}{2}u(1-u^2) + \chi w + \varepsilon G(s) \\
 \dot{w} &= -\lambda w - \kappa(y+v) \\
 \dot{s} &= 1,
 \end{aligned} \tag{1}$$

where  $G(s)$  is a  $T$ -periodic forcing,  $\lambda$  is a time constant of the electrical circuit and  $\chi$  and  $\kappa$  are the dimensionless piezoelectric couplings in the mechanical and electrical equations, respectively. Note that these are indeed the equations for the coupling of two identical piezoelectric beams. If they are different one just needs to consider different parameters  $\chi_i$  and  $\zeta_i$ , but essentially everything that follows holds the same.

Let us now assume that the damping ( $\zeta$ ), the piezoelectric couplings ( $\chi$  and  $\kappa$ )

and the amplitude of the external forcing are small. We can then introduce a perturbation parameter,  $\varepsilon > 0$ , and, after performing the scaling

$$\zeta = \varepsilon\tilde{\zeta}, \quad \chi = \varepsilon\tilde{\chi} \quad (2)$$

we can write the system as

$$\dot{\tilde{z}} = g_0(\tilde{z}) + \varepsilon g_1(\tilde{z}) \quad (3)$$

where  $\tilde{z} = (x, y, u, v, w, s) \in \mathbb{R}^5 \times \mathbb{T}_T = \mathbb{R}^5 \times \mathbb{R}/T\mathbb{Z}$ ,

$$g_0(\tilde{z}) = \begin{pmatrix} y \\ \frac{1}{2}x(1-x^2) \\ v \\ \frac{1}{2}u(1-u^2) \\ -\lambda w - k(y+v) \\ 1 \end{pmatrix}$$

and

$$g_1(\tilde{z}) = \begin{pmatrix} 0 \\ -2\tilde{\zeta}y + \tilde{\chi}w + G(s) \\ 0 \\ -2\tilde{\zeta}v + \tilde{\chi}w + G(s) \\ 0 \\ 0 \end{pmatrix} \quad (4)$$

The unperturbed system,

$$\dot{\tilde{z}} = g_0(\tilde{z}) \quad (5)$$

consists of two uncoupled systems, one for each beam in  $\mathbb{R}^2$ , the equation for  $\dot{w}$  describing the piezoelectric coupling and the time evolution  $\dot{s} = 1$ . Each of the systems describing the motion of the beams (see [23]) is Hamiltonian,

$$\begin{aligned} \mathcal{X}(x, y) &= \frac{y^2}{2} - \frac{1}{4}x^2 \left(1 - \frac{x^2}{2}\right) \\ \mathcal{U}(u, v) &= \frac{v^2}{2} - \frac{1}{4}u^2 \left(1 - \frac{u^2}{2}\right). \end{aligned}$$

The phase portrait for each of oscillator is shown in Figure 3 and consists of a figure of eight. It posses three equilibrium points:

$$\begin{aligned} Q^\pm &= (\pm 1, 0) \\ Q_0 &= (0, 0). \end{aligned}$$

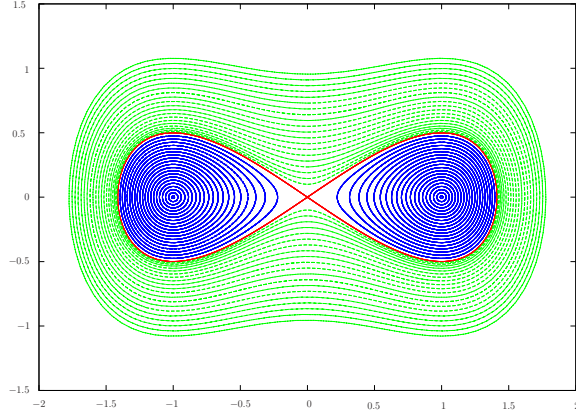


Figure 3: Phase portrait of each beam in absence of forcing, damping and coupling.

The origin  $Q_0$  is a saddle point with two eight-figured homoclinic loops,

$$\gamma^\pm := \mathcal{W}^s(Q_0) \cap \mathcal{W}^u(Q_0) = \mathcal{W}^s(Q_0) = \mathcal{W}^u(Q_0), \quad (6)$$

such that

$$\gamma^+ \cup \{Q_0\} \cup \gamma^- = \{(x, y) \in \mathbb{R}^2, \mathcal{X}(x, y) = 0\}.$$

We consider parametrizations

$$\gamma^\pm = \{\sigma^\pm(t), t \in \mathbb{R}\} \quad (7)$$

satisfying

$$\begin{aligned} \lim_{t \rightarrow \pm\infty} \sigma^\pm(t) &= Q_0 \\ \sigma^\pm(0) &= (0, \pm\sqrt{2}). \end{aligned}$$

Each homoclinic loop  $\gamma^\pm$  surrounds the equilibrium point  $Q^\pm$ . The points  $Q^\pm$  are elliptic points, and the region bounded by the homoclinic loops are covered by periodic orbits.

For our construction, we will be interested in the higher energy periodic orbits located outside the homoclinic loops for system  $\mathcal{U}$

$$\mathcal{P}^c = \{(u, v) \in \mathbb{R}^2, |\mathcal{U}(u, v) = c\}, \quad (8)$$

with  $c > 0$ , while system  $\mathcal{X}$  remains close to the hyperbolic point  $Q_0$ . Similar invariant objects to the ones we will construct can be obtained when

focusing on the two type of periodic orbits inside the homoclinic loops and surrounding each of the elliptic points  $Q^\pm$ .

The periods of the periodic orbits  $\mathcal{P}^c$  can be computed as follows. Consider the periodic orbit with initial condition  $(0, v_0)$ , with level of energy

$$c = \frac{v_0^2}{2},$$

which crosses the  $u$  axis at the point

$$(u_1, 0) = \left( \sqrt{1 + \sqrt{1 + 8c}}, 0 \right).$$

Using the symmetries of the system and its Hamiltonian structure, we obtain that the period of a periodic orbit  $\mathcal{P}^c$ , with  $c = \frac{v_0^2}{2}$ , becomes

$$\begin{aligned} \alpha(c) &:= 4 \int_0^{u_1} \frac{1}{\dot{u}} du \\ &= 4 \int_0^{u_1} \frac{1}{\sqrt{2c + \frac{u^2}{2} \left(1 - \frac{u^2}{2}\right)}} du. \end{aligned} \quad (9)$$

We now focus on the dynamics restricted to these periodic orbits for system  $\mathcal{U}$  while systems  $\mathcal{X}$  remains at its equilibrium point  $Q_0$ . Provided that each of these periodic orbits is contained in the energy level given by  $\mathcal{U}(u, v) = c$ , it will be more natural to parametrize them by  $c$  and an angle,  $\theta$ . Hence we will consider “action angle”-like variables  $(\theta, c) \in \mathbb{T} \times \mathbb{R}$  to parametrize periodic orbits  $\mathcal{P}^c$  as follows. Letting  $\varphi_{\mathcal{U}}(t; u_0, v_0)$  be the flow associated with system  $\mathcal{U}$  such that  $\varphi_{\mathcal{U}}(0; u_0, v_0) = (u_0, v_0)$ , we consider

$$\begin{aligned} p : \mathbb{T} \times \mathbb{R} &\longrightarrow \mathbb{R}^2 \\ (\theta, c) &\longmapsto \varphi_{\mathcal{U}}(\theta\alpha(c); 0, \sqrt{2c}). \end{aligned} \quad (10)$$

Note that this induces the dynamics

$$\begin{aligned} \dot{\theta} &= \frac{1}{\alpha(c)} \\ \dot{c} &= 0. \end{aligned}$$

When  $(x, y) = Q_0$ , provided that  $\lambda > 0$ , the variable  $w$  is attracted to a certain object given by the dynamics of  $v$ . Writing

$$v^p(t; u_0, v_0) = \Pi_v(\varphi_{\mathcal{U}}(t; u_0, v_0)), \quad (11)$$

the dynamics of  $w$  restricted to  $(x, y) = Q_0 = (0, 0)$  is given by

$$\dot{w} = -\lambda w - kv^p(t). \quad (12)$$

Provided that for  $k = 0$  Equation (12) is linear and that  $v_p(t)$  is  $\alpha(c)$ -periodic, the  $\alpha(c)$ -time return map associated with system (12) possesses a fixed point for any value of  $k$  and, hence, system (12) possesses an  $\alpha(c)$ -periodic orbit:

$$w^p(t + \alpha(c)) = w^p(t),$$

which is attracting.

Let us now compute the initial condition for such periodic orbit. Note that, although system (12) is not autonomous, we can assume that the initial conditions are given for  $t = 0$ , since Equation (12) has to be integrated together with the equations for  $\dot{u}$  and  $\dot{v}$ , forming an autonomous system. Therefore, the general solution of (12) becomes

$$w(t; w_0) = e^{-\lambda t} \left( \int_0^t -kv^p(s)e^{\lambda s} ds + w_0 \right),$$

from where, imposing  $w(\alpha(c); w_0) = w_0$ , we get that the initial condition for a periodic orbit is

$$w_0^p = \frac{e^{-\lambda\alpha(c)}}{1 - e^{-\lambda\alpha(c)}} \int_0^{\alpha(c)} -kv^p(s)e^{\lambda s} ds.$$

Hence, given  $(u_0, v_0)$ , the attracting periodic orbit of  $w$  becomes

$$w^p(t) = e^{-\lambda t} \left( \int_0^t -kv^p(s)e^{\lambda s} ds + \frac{e^{-\lambda\alpha(c)}}{1 - e^{-\lambda\alpha(c)}} \int_0^{\alpha(c)} -kv^p(s)e^{\lambda s} ds \right).$$

Note that  $w_0^p$  depends on  $u_0$  and  $v_0$  through the periodic orbit (11). To emphasize it, we will write  $w_0^p(u_0, v_0)$ . Note that  $w_0^p(u_0, v_0)$  is indeed a parametrization of the whole periodic orbit  $w^p(t)$ , just by keeping  $t = 0$  and varying  $u, v$  along the periodic orbit  $\mathcal{P}_c$ . Hence we have obtained the 3-dimensional invariant manifold

$$\tilde{\mathcal{K}} = Q_0 \times \left( \bigcup_{c_1 \leq c \leq c_2} \left\{ (u, v, w) \mid \mathcal{U}(u, v) = c, w = w_0^p(u, v) \right\} \right) \times \mathbb{T}_T \subset \mathbb{R}^5 \times \mathbb{T}_T.$$

Recalling that  $(u_0, v_0)$  can be parametrized by  $p(\theta, c)$ ,  $w_0^p$  can be as well parametrized by  $\theta$  and  $c$ :  $w_0^p = w_0^p(p(\theta, c))$ . This induces a parametrization for  $\tilde{\mathcal{K}}$

$$\tilde{K} : \mathbb{T} \times \mathbb{R} \times \mathbb{T}_T \longrightarrow \mathbb{R}^5 \times \mathbb{T}_T, \quad (13)$$

given by

$$\tilde{K}(\theta, c, s) = \begin{pmatrix} 0 \\ 0 \\ p(\theta, c) \\ w_0^p(p(\theta, c)) \\ s \end{pmatrix} \quad (14)$$

and hence

$$\tilde{\mathcal{K}} = \tilde{K}(\mathbb{T}, [c_1, c_2], \mathbb{T}_T),$$

The invariant manifold  $\tilde{\mathcal{K}}$  is foliated by 2-dimensional invariant tori contained at energy level  $c$ :

$$\tilde{\mathcal{K}} = Q_0 \times \bigcup_{c_1 \leq c \leq c_2} \tilde{\mathcal{K}}^c.$$

Each of these tori is homeomorphic to  $\mathbb{T} \times \mathbb{T}_T$ ,

$$\tilde{\mathcal{K}}^c \simeq \mathbb{T} \times \mathbb{T}_T,$$

as it can be parametrized by  $(\theta, s)$ :

$$\tilde{\mathcal{K}}^c = \tilde{K}^c(\mathbb{T}, c, \mathbb{T}_T),$$

where

$$\tilde{K}^c : \mathbb{T} \times \mathbb{T}_T \longrightarrow \mathbb{R}^3 \times \mathbb{T}_T \quad (15)$$

and

$$\begin{aligned} \tilde{K}^c(\theta, s) &= \Pi_{u,v,w,s} \left( \tilde{K}(\theta, c, s) \right) \\ &= (p(\theta, c), w_0^p(p(\theta, c)), s) \end{aligned}$$

When  $c$  is such that  $T$  and  $\alpha(c)$  are congruent, then  $\tilde{\mathcal{K}}^c$  is filled by periodic orbits: each point is a periodic point of the  $T$ -time return map. However, when  $T$  and  $\alpha(c)$  are incommensurable,  $\tilde{\mathcal{K}}^c$  is densely filled by any solution with initial conditions at  $\tilde{\mathcal{K}}^c$ . Note that this implies that, for any initial condition at the invariant manifold  $\tilde{\mathcal{K}}$ , one obtains bounded dynamics both for  $t \rightarrow \infty$  and  $t \rightarrow -\infty$ .

We now show that the invariant manifold  $\tilde{\mathcal{K}}$  is normally hyperbolic (NHIM), by showing that it has stable/unstable normal bundles with exponential convergence/divergence.

The hyperbolicity is inherited from the hyperbolic point  $Q_0$ . We consider  $(x, y)$  coordinates at one of the homoclinic loops of  $Q_0$  parametrized by  $\tau$ :

$$\sigma(\tau) \in \gamma, \quad (16)$$

where  $\sigma(\tau)$  can be either  $\sigma^+(\tau)$  or  $\sigma^-(\tau)$  (similarly for  $\gamma$ ). We also fix parameters  $\theta, c$  and  $s$  leading to a point

$$\tilde{K}^c(\theta, s) = (u, v, w, s) \in \tilde{\mathcal{K}}^c. \quad (17)$$

Letting  $\varphi_{\mathcal{X}}(t; x, y)$  be the flow associated with the Hamiltonian  $\mathcal{X}$ , we call

$$y^h(t; \tau) = \Pi_y(\varphi_{\mathcal{X}}(t; \sigma(\tau))).$$

We may omit explicit dependence of  $y^h$  on  $\tau$ .

When restricted to the conditions (16)-(17), the variable  $w$  evolves following the equation

$$\dot{w} = -\lambda w - k(y^h(t) + v^p(t)), \quad (18)$$

which has the general solution

$$w(t) = e^{-\lambda t} \left( w_0 - \int_0^t k(y^h(s) + v^p(s)) e^{\lambda s} ds \right). \quad (19)$$

Then, the stable and unstable manifolds  $\mathcal{W}^s(\tilde{\mathcal{K}})$  and  $\mathcal{W}^u(\tilde{\mathcal{K}})$  will be given by (16)-(17) and solutions of (19) satisfying

$$\lim_{t \rightarrow \infty} |w^s(t) - w^p(t)| \rightarrow 0$$

and

$$\lim_{t \rightarrow -\infty} |w^u(t) - w^p(t)| \rightarrow 0.$$

In order to find  $w^u(0)$  and  $w^s(0)$ , let us define

$$z(t) = w(t) - w^p(t) = e^{-\lambda t} \left( z_0 - \int_0^t k y^h(s) e^{\lambda s} ds \right),$$

where

$$z_0 = w(0) - w^p(0). \quad (20)$$

Due to the hyperbolicity of  $Q_0$ , we know that there exist positive constants  $\tilde{\lambda}, M$  and  $\delta$  such that

$$|y^h(t) - 0| < M e^{-\tilde{\lambda}|t|}, \quad |t| > \delta$$

Hence, we get that

$$\begin{aligned}\lim_{t \rightarrow +\infty} |z(t)| &= \lim_{t \rightarrow +\infty} \left( e^{-\lambda t} z_0 - \int_0^t k y^h(s) e^{\lambda(s-t)} ds \right) \\ &< \lim_{t \rightarrow +\infty} \int_0^t k e^{-\bar{\lambda}s + \lambda(s-t)} ds = 0,\end{aligned}$$

for any  $z_0 \in \mathbb{R}$ , and all initial conditions for  $w$  are attracted to the periodic orbit  $w^p(t)$ .

However, the limit for  $t \rightarrow -\infty$  diverges unless we choose

$$z_0 = - \int_{-\infty}^0 k e^{\lambda s} y^h(s) ds.$$

In this case, we get

$$\begin{aligned}\lim_{t \rightarrow -\infty} |z(t)| &= \lim_{t \rightarrow -\infty} \left| e^{-\lambda t} \left( \int_{-\infty}^0 k e^{\lambda s} y^h(s) ds + \int_0^t k e^{\lambda s} y^h(s) ds \right) \right| \\ &= \lim_{t \rightarrow -\infty} \left| e^{-\lambda t} \int_{-\infty}^t k e^{\lambda s} y^h(s) ds \right| \\ &< \lim_{t \rightarrow -\infty} \left| e^{-\lambda t} \int_{-\infty}^t k M e^{(\lambda + \bar{\lambda})s} ds \right| \\ &= \lim_{t \rightarrow -\infty} \frac{k M e^{\bar{\lambda}t}}{\lambda + \bar{\lambda}} = 0.\end{aligned}$$

Note that the manifolds  $\mathcal{W}^s(\tilde{\mathcal{K}})$  and  $\mathcal{W}^u(\tilde{\mathcal{K}})$  locally generate the normal bundle to  $\tilde{\mathcal{K}}$ , as they generate the  $x - y$  plane and the stable manifold contains the hyperplane  $w$ . Therefore, and summarizing, we have proven the following result.

**Lemma 1.** *System (5) possesses a foliated 3-dimensional invariant manifold*

$$\tilde{\mathcal{K}} = Q_0 \times \bigcup_{c_1 \leq c \leq c_2} \tilde{\mathcal{K}}^c$$

with

$$\begin{aligned}\tilde{\mathcal{K}}^c &= \left\{ (u, v, w, s) \in \mathcal{P}_c \times \mathbb{R} \times \mathbb{T}_T, | w = w_0^p(u, v) \right\} \\ \mathcal{P}_c &= \left\{ (u, v) \in \mathbb{R}^2, | \mathcal{U}(u, v) = c \right\} \\ w_0^p(u, v) &= \frac{e^{-\lambda\alpha(c)}}{1 - e^{-\lambda\alpha(c)}} \int_0^{\alpha(c)} -k v^p(s; u, v) e^{\lambda s} ds \\ v^p(s; u, v) &= \Pi_v(\varphi_{\mathcal{U}}(s; u, v)).\end{aligned}\tag{21}$$

The manifold  $\tilde{\mathcal{K}}$  is normally hyperbolic, has a 5-dimensional stable manifold

$$\mathcal{W}^s(\tilde{\mathcal{K}}) = \mathcal{W}^s(Q_0) \times \bigcup_{c \in [c_1, c_2]} \mathcal{P}_c \times \mathbb{R} \times \mathbb{T}_T$$

and a 4-dimensional unstable manifold given by the union of two homoclinic loops,

$$\mathcal{W}^u(\tilde{\mathcal{K}}) = \tilde{\Gamma}^+ \cup \tilde{\Gamma}^- \subset \mathcal{W}^s(\tilde{\mathcal{K}}),$$

where

$$\begin{aligned} \tilde{\Gamma}^+ &= \bigcup_{c_1 \leq c \leq c_2} \left\{ (x, y, u, v, w, s) \in \gamma^+ \times \mathcal{P}_c \times \mathbb{R} \times \mathbb{T}_T, \right. \\ &\quad \left. w = w_0^u(x, y, u, v) \right\} \\ \tilde{\Gamma}^- &= \bigcup_{c_1 \leq c \leq c_2} \left\{ (x, y, u, v, w, s) \in \gamma^- \times \mathcal{P}_c \times \mathbb{R} \times \mathbb{T}_T, \right. \\ &\quad \left. w = w_0^u(x, y, u, v) \right\} \end{aligned}$$

and

$$\begin{aligned} w_0^u(x, y, u, v) &= - \int_{-\infty}^0 k e^{\lambda s} y^h(s; x, y) ds + w_0^p(u, v) \quad (22) \\ y^h(s; x, y) &= \Pi_y(\varphi_{\mathcal{X}}(s; x, y)) \\ (x, y) &\in \gamma^+ \cup \gamma^-. \end{aligned}$$

There exist parametrizations such that these manifolds can be written as

$$\begin{aligned} \mathcal{P}_c &= p(\mathbb{T}, c) \\ \tilde{\mathcal{K}}^c &= \tilde{K}^c(\mathbb{T}, \mathbb{T}_T) \\ \tilde{\mathcal{K}} &= \tilde{K}(\mathbb{T}, [c_1, c_2], \mathbb{T}_T) \\ \mathcal{W}^s(\tilde{\mathcal{K}}) &= \tilde{W}^{s,+}(\mathbb{T}, [c_1, c_2], \mathbb{T}_T, \mathbb{R}^2) \\ &\quad \cup \tilde{W}^{s,-}(\mathbb{T}, [c_1, c_2], \mathbb{T}_T, \mathbb{R}^2) \\ \mathcal{W}^u(\tilde{\mathcal{K}}) &= \tilde{W}^{u,+}(\mathbb{T}, [c_1, c_2], \mathbb{T}_T, \mathbb{R}) \\ &\quad \cup \tilde{W}^{u,-}(\mathbb{T}, [c_1, c_2], \mathbb{T}_T, \mathbb{R}) \end{aligned}$$

where

$$\begin{aligned} p: \mathbb{T} \times (0, \infty) &\longrightarrow \mathbb{R}^2 \\ (\theta, c) &\longmapsto \varphi_U(\theta \alpha(c); 0, \sqrt{2c}) \end{aligned}$$

$$\begin{aligned}
\tilde{K}^c : \mathbb{T} \times \mathbb{T}_T &\longrightarrow \mathbb{R}^3 \times \mathbb{T}_T \\
(\theta, s) &\longmapsto (p(\theta, c), w_0^p(p(\theta, c)), s) \\
\tilde{K} : \mathbb{T} \times \mathbb{R} \times \mathbb{T}_T &\longrightarrow \mathbb{R}^5 \times \mathbb{T}_T \\
(\theta, c, s) &\longmapsto (0, 0, \tilde{K}_0^c(\theta, s)) \\
\tilde{W}^{s,\pm} : \mathbb{T} \times [c_1, c_2] \times \mathbb{T}_T \times \mathbb{R}^2 &\longrightarrow \mathbb{R}^5 \times \mathbb{T}_T \\
(\theta, c, s, \tau, r) &\longmapsto (\sigma^\pm(\tau), p(\theta, c), r, s) \\
\tilde{W}^{u,\pm} : \mathbb{T} \times [c_1, c_2] \times \mathbb{T}_T \times \mathbb{R} &\longrightarrow \mathbb{R}^5 \times \mathbb{T}_T \\
(\theta, c, s, \tau) &\longmapsto (\sigma^\pm(\tau), p(\theta, c), w_0^u(\sigma^\pm(\tau), p(\theta, c)), s)
\end{aligned}$$

## 2.2 Persistence of manifolds

For  $\varepsilon > 0$  theory of normally hyperbolic invariant manifolds (see [13]) guarantees that (locally) there exists  $\tilde{\mathcal{K}}_\varepsilon$   $\varepsilon$ -close to  $\tilde{\mathcal{K}}$ , with  $\tilde{\mathcal{K}}_0 = \tilde{\mathcal{K}}$ . However, in the case of considering only the perturbation given by the external forcing ( $\varepsilon > 0$  and  $\tilde{\zeta} = \tilde{\chi} = 0$ ), the perturbation is Hamiltonian. Hence, as the system remains uncoupled, the inner dynamics is symplectic and KAM Theorem ([6]) holds. This guarantees that, those periodic orbits whose periods are, modulo  $T$ , away enough from rational numbers, persist as invariant tori. Hence, in the Hamiltonian case, this manifold  $\tilde{\mathcal{K}}_\varepsilon$  is a manifold with boundaries and hence it becomes a globally unique invariant manifold. Indeed we will assume that the curves  $c = c_1$  and  $c = c_2$  parametrize two invariant tori consisting of the lower and upper boundaries of the manifold.

When the perturbation includes dissipative terms ( $\tilde{\zeta} > 0$  and/or  $\tilde{\chi} > 0$ ), the existence of these boundaries is not guaranteed. Indeed, as it will be shown in Section 4, the inner dynamics contains a global attractor in either case. As a consequence of that, KAM tori do not necessarily persist and  $\tilde{\mathcal{K}}_\varepsilon$  becomes a manifold without boundaries. Therefore, theory for normally hyperbolic manifolds can only guaranty its local uniqueness. To show the existence of unique manifold  $\tilde{\mathcal{K}}_\varepsilon$  for  $\varepsilon > 0$  small enough, we argue as follows. We consider  $[c'_1, c'_2]$  such that  $[c_1, c_2] \subset [c'_1, c'_2]$  and construct a new smooth field  $g'_\varepsilon(\tilde{z})$  which coincides with our field  $g_0(\tilde{z}) + \varepsilon g_1(\tilde{z})$  for  $c \in (c'_1, c'_2)$  and vanishes otherwise. Hence we can use theory for normally hyperbolic invariant manifolds to obtain the persistence of a globally unique “larger” manifold  $\tilde{\mathcal{K}}'_\varepsilon$  invariant under  $g'_\varepsilon$ ,  $\varepsilon$ -close to  $K(\mathbb{T}_T, [c'_1, c'_2], \mathbb{T})$  and whose dynamics does not leave  $\tilde{\mathcal{K}}'_\varepsilon$ . As  $\tilde{\mathcal{K}}_\varepsilon \subset \tilde{\mathcal{K}}'_\varepsilon$  and  $g'_\varepsilon$  coincides with  $g_0 + \varepsilon g_1$  in  $\tilde{\mathcal{K}}'_\varepsilon$ , the manifold  $\tilde{\mathcal{K}}_\varepsilon$  is also unique. However, the dynamics of  $g_0(\tilde{z}) + \varepsilon g_1(\tilde{z})$ , coinciding with the one of  $g'_\varepsilon$  in  $\tilde{\mathcal{K}}'_\varepsilon$ , may leave  $\tilde{\mathcal{K}}_\varepsilon$ . This however occurs

slowly and points away from original boundaries  $c = c_1$  and  $c = c_2$  remain in  $\tilde{\mathcal{K}}_\varepsilon$  for large periods of time.

Hence we have parameterizations

$$\tilde{K}_\varepsilon : \mathbb{T} \times [c_1, c_2] \times \mathbb{T}_T \longrightarrow \mathbb{R}^5 \times \mathbb{T}_T \quad (23)$$

$$\tilde{W}_\varepsilon^{s,\pm} : \mathbb{T} \times [c_1, c_2] \times \mathbb{T}_T \times \mathbb{R}^2 \longrightarrow \mathbb{R}^5 \times \mathbb{T}_T \quad (24)$$

$$\tilde{W}_\varepsilon^{u,\pm} : \mathbb{T} \times [c_1, c_2] \times \mathbb{T}_T \times \mathbb{R} \longrightarrow \mathbb{R}^5 \times \mathbb{T}_T \quad (25)$$

such that the manifolds

$$\begin{aligned} \tilde{\mathcal{K}}_\varepsilon &= \tilde{K}_\varepsilon(\mathbb{T}, [c_1, c_2], \mathbb{T}_T) \\ \mathcal{W}^s(\tilde{\mathcal{K}}_\varepsilon) &= \tilde{W}_\varepsilon^{s,+}(\mathbb{T}, [c_1, c_2], \mathbb{T}_T, \mathbb{R}^2) \\ &\quad \cup \tilde{W}_\varepsilon^{s,-}(\mathbb{T}, [c_1, c_2], \mathbb{T}_T, \mathbb{R}^2) \\ \mathcal{W}^u(\tilde{\mathcal{K}}_\varepsilon) &= \tilde{W}_\varepsilon^{u,+}(\mathbb{T}, [c_1, c_2], \mathbb{T}_T, \mathbb{R}) \\ &\quad \cup \tilde{W}_\varepsilon^{u,-}(\mathbb{T}, [c_1, c_2], \mathbb{T}_T, \mathbb{R}) \end{aligned}$$

are unique and locally invariant.

These parameterizations, together with the dynamics of the system restricted to  $\tilde{\mathcal{K}}_\varepsilon$  and linear approximations of the manifolds  $\mathcal{W}_\varepsilon^s(\tilde{\mathcal{K}}_\varepsilon)$  and  $\mathcal{W}_\varepsilon^u(\tilde{\mathcal{K}}_\varepsilon)$  will be numerically computed in Section 3 by means of the parameterization method.

### 3 Numerical framework for the parameterization method

In this section we numerically compute the perturbed Normally Hyperbolic Manifold  $\tilde{\mathcal{K}}_\varepsilon$  by means of the so-called parameterization method, introduced in [3, 4, 5].

The parameterization method is stated easier when formulated for maps; hence, it will be more convenient to write the full system (3) as discrete system. The most natural map to consider is of course the stroboscopic map, due to the periodicity of the system. However, due to the foliated nature of the unperturbed manifold  $\tilde{\mathcal{K}}_0$ , instead of using the original variables, we will consider from now on the induced map in the manifolds introduced in Section 2.1:

$$\begin{aligned} F_\varepsilon : \mathbb{T} \times (0, \infty) \times \mathbb{R}^3 &\longrightarrow \mathbb{T} \times (0, \infty) \times \mathbb{R}^3 \\ (\theta, c, x, y, w) &\longmapsto \tilde{p} \circ \mathfrak{s}_\varepsilon \circ \tilde{p}^{-1}(\theta, c, x, y, w), \end{aligned} \quad (26)$$

where  $\tilde{p}$  is the change of variables

$$\tilde{p}(\theta, c, x, y, w) = (x, y, p(\theta, c), w) = (x, y, \varphi_{\mathcal{U}}(\theta\alpha(c); 0, \sqrt{2c}), w)$$

and  $\mathfrak{s}_\varepsilon$  is the stroboscopic map

$$\begin{aligned} \mathfrak{s}_\varepsilon : \quad \Sigma_{s_0} &\longrightarrow \Sigma_{s_0} \\ (x, y, u, v, w) &\longmapsto \tilde{\phi}_\varepsilon(s_0 + T; x, y, u, v, w, s). \end{aligned}$$

Arguing as in Section 2.2, by considering the flow  $g'$  we obtain a map  $F'_\varepsilon$  and a parameterization

$$K_\varepsilon : \mathbb{T} \times [c'_1, c'_2] \longrightarrow \mathbb{T} \times [c'_1, c'_2] \times \mathbb{R}^3, \quad (27)$$

such that the manifold

$$\mathcal{K}'_\varepsilon = K_\varepsilon(\mathbb{T} \times [c'_1, c'_2])$$

is unique, normally hyperbolic and invariant under  $F'_\varepsilon$ . Moreover,  $F'_\varepsilon$  and  $F_\varepsilon$  coincide in  $\mathcal{K}'_\varepsilon$ . By restricting the parameterization  $K_\varepsilon$  to  $[c_1, c_2]$ , we obtain a manifold,

$$\mathcal{K}_\varepsilon = K_\varepsilon(\mathbb{T}, [c_1, c_2]),$$

which is unique and normally hyperbolic. Although it is locally invariant,  $\mathcal{K}_\varepsilon$  contains the image of those points isolated enough from the boundaries of  $\mathcal{K}_0$  ( $c = c_1$  and  $c = c_2$ ).

The map  $F_\varepsilon$  restricted to  $\mathcal{K}_\varepsilon$  induces inner dynamics in  $\mathcal{K}_\varepsilon$  given by a map

$$f_\varepsilon : \mathbb{T} \times [c_1, c_2] \longrightarrow \mathbb{T} \times [c'_1, c'_2].$$

We find the inner dynamics  $f_\varepsilon$  and the parameterization  $K_\varepsilon$ , using the parameterization, that is, by imposing that the diagram

$$\begin{array}{ccc} \mathbb{T} \times [c_1, c_2] & \xrightarrow{K_\varepsilon} & \mathbb{T} \times [c_1, c_2] \times \mathbb{R}^3 \\ \downarrow f_\varepsilon & & \downarrow F_\varepsilon \\ \mathbb{T} \times [c'_1, c'_2] & \xrightarrow{K_\varepsilon} & \mathbb{T} \times [c'_1, c'_2] \times \mathbb{R}^3 \end{array}$$

commutes.

Note that, although we do not have an explicit expression for the map  $F_\varepsilon$ , we can consider that it is given provided that we can numerically compute the stroboscopic map  $\mathfrak{s}$  just by integrating the system. Hence, we need to solve the cohomological

$$F_\varepsilon \circ K_\varepsilon - K_\varepsilon \circ f_\varepsilon = 0 \quad (28)$$

for the unknowns  $f_\varepsilon$  and  $K_\varepsilon$ . We do this by following the method described in [18] (Chapter 5). It consists of taken advantage of the hyperbolicity of  $\mathcal{K}_\varepsilon$  to perform a Newton-like method to compute functions  $f_\varepsilon$  and  $K_\varepsilon$ . In practice, given a discretization of the reference manifold  $\mathbb{T}_T \times [c_1, c_2]$ , this means that we want to compute the coefficients for approximations (splines, Fourier series or Lagrangian polynomials) of  $f_\varepsilon$  and  $K_\varepsilon$ . We first review the method described in [18] adapted to our case.

### 3.1 A Newton-like method

Assume that, for a certain  $\varepsilon > 0$ , we have good enough approximations of  $K_\varepsilon$  and  $f_\varepsilon$ . As usual in Newton-like methods, in order to provide improved approximations, we will require as well an initial guess of the dynamics at the tangent bundles; that is, approximations of the solutions to the cohomological equation

$$DF_\varepsilon(K_\varepsilon(\theta, c)) - DK_\varepsilon(f_\varepsilon(\theta, c)) = 0. \quad (29)$$

Note that Equation (29) manifests the invariance of the tangent bundle  $TK_\varepsilon$  under  $DF_\varepsilon$ , leading to inner dynamics at  $TK_\varepsilon$  given by  $Df_\varepsilon$ . However,  $DF_\varepsilon$  is a map onto the tangent space  $T(\mathbb{T} \times \mathbb{R} \times \mathbb{R}^3)$ . The latter can be generated by two vectors in  $TK_\varepsilon$  and three in the normal bundle  $NK_\varepsilon$ ,  $T(\mathbb{T} \times \mathbb{R} \times \mathbb{R}^3) = TK_\varepsilon \times NK_\varepsilon$ . Provided that  $\mathcal{K}_\varepsilon$  is normally hyperbolic, the normal space  $NK_\varepsilon$  can be generated by two vectors tangent to  $\mathcal{W}^s(\mathcal{K}_\varepsilon)$  and a third one tangent to  $\mathcal{W}^u(\mathcal{K}_\varepsilon)$ . It will be hence useful to consider the adapted frame around  $\mathcal{K}_\varepsilon$

$$P_\varepsilon(\theta, c) = (L_\varepsilon(\theta, c) N_\varepsilon(\theta, c)),$$

given by the juxtaposition of the matrices  $L_\varepsilon$  and  $N_\varepsilon$ , where

$$L_\varepsilon(\theta, c) = DK_\varepsilon(\theta, c)$$

is a  $5 \times 2$  matrix and  $N_\varepsilon(\theta, c)$  is  $5 \times 3$  given by the three columns of  $DF_\varepsilon$  generating the normal bundle  $NK_\varepsilon$ .

The matrix  $P_\varepsilon$  can be seen as a change of basis such that the skew product

$$(f_\varepsilon, \Lambda_\varepsilon) : \mathbb{T} \times [c_1, c_2] \times \mathbb{R}^5 \longrightarrow \mathbb{T} \times [c_1, c_2] \times \mathbb{R}^5,$$

with

$$\Lambda_\varepsilon = P_\varepsilon(f(\theta, c))^{-1} DF_\varepsilon(K_\varepsilon(\theta, c)) P_\varepsilon(\theta, c),$$

becomes of the form

$$\Lambda_\varepsilon = \begin{pmatrix} \Lambda_\varepsilon^L & 0 & 0 & 0 \\ \Lambda_\varepsilon^L & 0 & 0 & 0 \\ 0 & 0 & \Lambda_\varepsilon^S & 0 \\ 0 & 0 & \Lambda_\varepsilon^S & 0 \\ 0 & 0 & 0 & 0 & \Lambda_\varepsilon^U \end{pmatrix}.$$

Note that

$$\Lambda_\varepsilon^L = Df_\varepsilon.$$

The Newton-like method consists of two steps. Given approximations of  $K_\varepsilon$  (and hence  $L_\varepsilon = DK_\varepsilon$ ),  $f_\varepsilon$  (and hence  $\Lambda_\varepsilon^L = Df_\varepsilon$ ),  $\Lambda_\varepsilon^S$  and  $\Lambda_\varepsilon^N$ , in the first step, one computes new corrected versions of  $K_\varepsilon$  and  $f_\varepsilon$  (and hence  $L_\varepsilon$  and  $\Lambda_\varepsilon^L$ ). In the second step, one corrects the normal bundle  $N_\varepsilon$  and its linearized dynamics  $\Lambda_\varepsilon^N$ .

### 3.1.1 First step: correction of the manifold and the inner dynamics

Following [18], we consider corrections of the form

$$\begin{aligned} \bar{f}_\varepsilon &= f_\varepsilon + \Delta f_\varepsilon \\ \bar{K}_\varepsilon &= K_\varepsilon + \Delta K_\varepsilon, \end{aligned}$$

with<sup>1</sup>

$$\Delta K_\varepsilon = P_\varepsilon(\theta, c)\zeta(\theta, c).$$

We want to compute  $\zeta(\theta, c)$  and  $\Delta f_\varepsilon(\theta, c)$ .

The corrections of the manifold,  $\zeta(\theta, c)$ , can be split in tangent, stable and unstable directions:

$$\zeta(\theta, c) = \begin{pmatrix} \zeta^L(\theta, c) \\ \zeta^S(\theta, c) \\ \zeta^U(\theta, c) \end{pmatrix} \in \mathbb{R}^2 \times \mathbb{R}^2 \times \mathbb{R}.$$

Let  $E(\theta, c)$  be the error at Equation (28) at the current value  $f_\varepsilon$  and  $K_\varepsilon$ ,

$$E(\theta, c) = F_\varepsilon(K_\varepsilon(\theta, c)) - K_\varepsilon(f_\varepsilon(\theta, c)).$$

---

<sup>1</sup>We permit ourselves here to keep the same notation as in the literature and call this correction  $\zeta$ . Although this coincides with the with the damping parameter from the original system (1), we believe that it will be clear from the context what we are referring to.

Let

$$\eta(\theta, c) = - (P(f(\theta, c)))^{-1} E(\theta, c),$$

which, again, we split in tangent, stable and unstable directions

$$\eta(\theta, c) = \begin{pmatrix} \eta^L(\theta, c) \\ \eta^S(\theta, c) \\ \eta^U(\theta, c) \end{pmatrix}.$$

Then, assuming that

$$\zeta^L(\theta, c) = \begin{pmatrix} 0 \\ 0 \end{pmatrix},$$

that is, the manifold  $K_\varepsilon(\mathbb{T}, [c_1, c_2])$  is only corrected in the normal directions,  $\Delta f_\varepsilon$  becomes

$$\Delta f_\varepsilon(\theta, c) = -\eta^L(\theta, c)$$

(see [18] for more details).

Regarding  $\Delta K_\varepsilon$ , by expanding Equation (28), one gets that  $\zeta^S$  and  $\zeta^U$  satisfy the equations

$$\eta^S(\theta, c) = \Lambda_\varepsilon^S(\theta, c)\zeta^S(\theta, c) - \zeta^S(\theta, c) \quad (30)$$

$$\eta^U(\theta, c) = \Lambda_\varepsilon^U(\theta, c)\zeta^U(\theta, c) - \zeta^U(\theta, c). \quad (31)$$

Due to hyperbolicity,  $\Lambda_\varepsilon^U > 1$  and the eigenvalues of  $\Lambda_\varepsilon^S$  are real, positive and inside the unite circle. Hence, Equations (30)-(31) can be solved by iterating the systems

$$\begin{aligned} \zeta^S(\theta, c) &= \Lambda_\varepsilon^S(f^{-1}(\theta, c))\zeta^S(f^{-1}(\theta, c)) - \eta^S(f^{-1}(\theta, c)) \\ \zeta^U(\theta, c) &= \frac{\zeta^U(f(\theta, c)) + \eta^U(\theta, c)}{\Lambda_\varepsilon^U(\theta, c)}. \end{aligned}$$

### 3.1.2 Second step: normal bundle correction

Once we have new corrected versions of the inner dynamics  $f_\varepsilon(\theta, c)$  (and consequently  $\Lambda_\varepsilon^L(\theta, c)$ ) and the parametrization  $K_\varepsilon(\theta, c)$  (and consequently  $L_\varepsilon(\theta, c)$ ), the second step consists of computing new approximations for  $\Lambda_\varepsilon^S$ ,  $\Lambda_\varepsilon^U$  and  $N_\varepsilon(\theta, c)$ . As in [18], we consider approximations of the form

$$\begin{aligned} \bar{N}_\varepsilon(\theta, c) &= N_\varepsilon(\theta, c) + \Delta N(\theta, c) \\ \bar{\Lambda}_\varepsilon^S(\theta, c) &= \Lambda_\varepsilon^S(\theta, c) + \Delta \Lambda^S(\theta, c) \\ \bar{\Lambda}_\varepsilon^U(\theta, c) &= \Lambda_\varepsilon^U(\theta, c) + \Delta \Lambda^U(\theta, c), \end{aligned}$$

with

$$\Delta N(\theta, c) = P_\varepsilon(\theta, c)Q^N(\theta, c).$$

Assuming that the corrections of the linearised stable and unstable bundles are applied only in the complementary directions, one gets that  $Q^N(\theta, c)$  is of the form

$$Q^N(\theta, c) = \begin{pmatrix} Q^{LS}(\theta, c) & Q^{LU}(\theta, c) \\ 0 & 0 & Q^{SU}(\theta, c) \\ 0 & 0 & \\ Q^{US}(\theta, c) & 0 \end{pmatrix}.$$

Let us write the current error in the cohomological equation at the tangent bundle (Equation (29)) as

$$E_{\text{red}}^N(\theta, c) = P_\varepsilon(\theta, c)^{-1}DF_\varepsilon(K_\varepsilon(\theta, c))N_\varepsilon(\theta, c) - \begin{pmatrix} 0 & 0 & 0 \\ 0 & 0 & 0 \\ \Lambda_\varepsilon^S(\theta, c) & 0 & 0 \\ 0 & 0 & \Lambda_\varepsilon^U(\theta, c) \end{pmatrix} = \begin{pmatrix} E_{\text{red}}^{LS}(\theta, c) & E_{\text{red}}^{LU}(\theta, c) \\ E_{\text{red}}^{SS}(\theta, c) & E_{\text{red}}^{SU}(\theta, c) \\ E_{\text{red}}^{US}(\theta, c) & E_{\text{red}}^{UU}(\theta, c) \end{pmatrix}$$

On one hand, the corrections of the adapted frame in the normal directions become

$$\begin{aligned} \Delta\Lambda^S(\theta, c) &= E_{\text{red}}^{SS}(\theta, c) \\ \Delta\Lambda^U(\theta, c) &= E_{\text{red}}^{UU}(\theta, c). \end{aligned}$$

On the other hand, the corrections of normal part of the change of basis  $P_\varepsilon(\theta, c)$ , are obtained by iterating the systems

$$\begin{aligned} Q^{LS}(\theta, c) &= (\Lambda_\varepsilon^L(\theta, c)) (Q^{LS}(f(\theta, c))\Lambda_\varepsilon^S(\theta, c) - E_{\text{red}}^{LS}(\theta, c)) \\ Q^{LU}(\theta, c) &= \frac{\Lambda_\varepsilon^L(f^{-1}(\theta, c)) + E_{\text{red}}^{LU}(f^{-1}(\theta, c))}{\Lambda_\varepsilon^U(f^{-1}(\theta, c))} \\ Q^{US}(\theta, c) &= \frac{Q^{US}(f(\theta, c))\Lambda_\varepsilon^S(\theta, c) - E_{\text{red}}^{US}(\theta, c)}{\Lambda_\varepsilon^U(\theta, c)} \\ Q^{SU}(\theta, c) &= \frac{\Lambda_\varepsilon^S(f^{-1}(\theta, c))Q^{SU}(f^{-1}(\theta, c)) + E_{\text{red}}^{SU}(f^{-1}(\theta, c))}{\Lambda_\varepsilon^U(f^{-1}(\theta, c))}. \end{aligned}$$

### 3.2 Computation of bundles, maps and frames for the unperturbed case

We now derive semi-explicit expressions for the objects for  $\varepsilon = 0$ :  $f_0(\theta, c)$ ,  $F_0(\theta, c, x, y, w)$ ,  $DF_0(\theta, c)$  and  $P_0(\theta, c)$ . The expressions below have to be partially solved numerically. By semi-explicit we mean that we will assume that computations such as numerical integration or differentiation is exact.

For  $\varepsilon = 0$ , the map  $F_0(\theta, c, x, y, w)$  consists of computing the stroboscopic map, integrating system (5), from  $t_0$  to  $t_0 + T$ . However, we first need to compute the change of variables  $p(\theta, c) = (u, v)$ , which requires the computation of  $\alpha(c)$ . Note that the expression provided in Equation (9) implies computing an improper integral provided that  $\dot{u} = 0$  at  $u = u_1$ , which is numerically problematic. Instead, we perform a Newton method to find the smallest  $t^* > 0$  such that

$$\Pi_u \left( \varphi_{\mathcal{U}}(t^*; 0, \sqrt{2c}) \right) = 0.$$

Then  $\alpha(c) = 2t^*$  due to the symmetry of the system. This is given by iterating the system

$$t_{i+1} = t_i - \frac{\Pi_u \left( \varphi_{\mathcal{U}}(t_i; 0, \sqrt{2c}) \right)}{\Pi_v \left( \varphi_{\mathcal{U}}(t_i; 0, \sqrt{2c}) \right)},$$

which allows to obtain a very accurate solution (precision around  $10^{-12}$  using order 7 – 8th order Runge Kutta integrator) in few iterations assuming that a good enough first guess is provided.

The stroboscopic map becomes

$$\mathfrak{s}_0(x, y, p(\theta, c), w) = \begin{pmatrix} \varphi_{\mathcal{X}}(T; x, y) \\ \varphi_{\mathcal{U}}(\theta\alpha(c) + T; 0, \sqrt{2c}) \\ w(T; w) \end{pmatrix},$$

where  $w(t; w)$  is the solution of equation

$$\dot{w} = -\lambda w - k(\Pi_y(\varphi_{\mathcal{X}}(t; x, y)) + \Pi_v(\varphi_{\mathcal{U}}(\tau; p(\theta, c)))). \quad (32)$$

Recall that, as mentioned in Section 2.1, Equation (32) can be seen as a one-dimensional non-autonomous differential equation, assuming that the flows  $\varphi_{\mathcal{X}}$  and  $\varphi_{\mathcal{U}}$  are known, but indeed depends on the initial values  $x, y, u, v$ .

Writing  $\mathfrak{s}$  in variables  $\theta, c$ , we obtain map the  $F_0$

$$F_0(\theta, c, x, y, w) = \begin{pmatrix} \theta + \frac{T}{\alpha(c)} \\ c \\ \varphi_{\mathcal{X}}(T; x, y) \\ w(T; w) \end{pmatrix},$$

and we assume that we can integrate system  $\mathcal{X}$  and Equation (32) “exactly”. For  $\varepsilon = 0$  the parameterization  $K_0(\theta, c)$  becomes

$$K_0(\theta, c) = \begin{pmatrix} \theta \\ c \\ 0 \\ 0 \\ w_0^p(p(\theta, c)) \end{pmatrix}.$$

Again, we need to compute  $w_0^p(p(\theta, c))$  numerically. One option is to numerically perform the integral given in Equation (21). However, it becomes faster and more precise to compute  $w_0^p(p(\theta, c))$  as the solution of a fixed point equation. Recall that, when restricted to the manifold  $\tilde{K}_0$ ,  $(x, y)$  are kept constant to  $(0, 0)$ , and hence the dynamics is given by system  $\mathcal{U}$  and  $\dot{w}$  as given in Equation (11), which we recall here for commodity

$$\left. \begin{aligned} \dot{u} &= v \\ \dot{v} &= \frac{1}{2}u(1 - u^2) \\ \dot{w} &= \lambda w - kv \end{aligned} \right\}. \quad (33)$$

Let  $\varphi_{\mathcal{U}w}(t; u, v, w)$  be the flow associated with system (33). Then,  $w_0^p(p(\theta, c))$  is the solution for  $w_0$  of the fixed point equation

$$\Pi_w(\varphi_{\mathcal{U}w}(\alpha(c); p(\theta, c), w_0)) - w_0 = 0, \quad (34)$$

which we can solve using a Newton method. Provided that  $\alpha(c)$  does not depend on  $w_0$ , the derivative  $\partial_{w_0}\Pi_w(\varphi_{\mathcal{U}w}(\alpha; p(\theta, c), w_0))$ , necessary for the Newton method, can be obtained by integrating the variational equations of system (33) from  $t = 0$  to  $t = \alpha(c)$ .

We next get

$$L_0(\theta, c) = DK_0(\theta, c) = \begin{pmatrix} 1 & 0 \\ 0 & 1 \\ 0 & 0 \\ 0 & 0 \\ \frac{\partial w_0^p(\theta, c)}{\partial \theta} & \frac{\partial w_0^p(\theta, c)}{\partial c} \end{pmatrix},$$

and we need to numerically compute the last row. Assuming that we have obtained  $w_0^p(p(\theta, c))$ , this can be done by applying the implicit function

theorem to Equation (34), which leads to

$$\begin{aligned} \frac{\partial w_0^p(p(\theta, c))}{\partial \theta} &= - \frac{\overbrace{D_{uv}\Pi_w(\varphi_{\mathcal{U}w}(\alpha(c); u, v, w_0^p(u, v)))}_{(u,v)=p(\theta,c)}^* \cdot D_\theta p(\theta, c)}{\underbrace{\partial_{w_0}\Pi_w(\varphi_{\mathcal{U}w}(\alpha(c); p(\theta, c), w_0))}_{w_0=w_0^p(\theta,c)} - 1}} \\ \frac{\partial w_0^p(p(\theta, c))}{\partial c} &= - \frac{\overbrace{\Pi_w(\varphi'_{\mathcal{U}w}(\alpha(c); p(\theta, c), w_0^p(p(\theta, c))))}_{-\lambda w_0^p(p(\theta,c))-k\Pi_v(p(\theta,c))} \cdot \alpha'(c)}{\partial_{w_0}\Pi_w(\varphi_{\mathcal{U}w}(\alpha(c); p(\theta, c), w_0))_{w_0=w_0^p(\theta,c)} - 1}} \\ &\quad - \frac{\overbrace{D_{uv}\varphi_{\mathcal{U}w}(\alpha(c); u, v, w_0^p(p(\theta, c)))}_{(u,v)=p(\theta,c)}^* \cdot D_c p(\theta, c)}{\underbrace{\partial_{w_0}\Pi_w(\varphi_{\mathcal{U}w}(\alpha(c); p(\theta, c), w_0))}_{w_0=w_0^p(\theta,c)} - 1}}. \end{aligned}$$

The terms labeled with \* can be obtained by integrating the variational equations of system (33), so we still need to obtain  $\alpha'(c)$  and  $D_{\theta c}p(\theta, c)$ . The former one is computed by finite differences provided that we can accurately compute  $\alpha_{c+h}$  and  $\alpha_{c-h}$  for a small enough  $h > 0$ . The latter becomes

$$\begin{aligned} Dp(\theta, c) &= D_{\theta,c}\varphi_{\mathcal{U}}(\theta\alpha(c); 0, \sqrt{2c}) \\ &= D_{uv}\varphi_{\mathcal{U}}(\theta\alpha(c); u, v)_{(u,v)=p(\theta,c)} \cdot \begin{pmatrix} 0 & 0 \\ 0 & \frac{1}{\sqrt{2c}} \end{pmatrix}, \end{aligned}$$

where  $D_{uv}\varphi_{\mathcal{U}}(\theta\alpha(c); u, v)$  can be obtained integrating the variational equations associated with system  $\mathcal{U}$ .

We now compute

$$DF_0(\theta, c, x, y, w) = \begin{pmatrix} -\frac{T}{\alpha(c)^2}\alpha'(c) & 1 & 0 & 0 & 0 \\ 0 & 1 & 0 & 0 & 0 \\ 0 & 0 & D_{xy}\varphi_{\mathcal{X}}(T; x, y) & 0 & 0 \\ 0 & 0 & 0 & 0 & 0 \\ \partial_\theta w' & \partial_c w' & \partial_x w' & \partial_y w' & \partial_w w' \end{pmatrix},$$

where  $w' = w(2\pi/\omega; w)$  is the solution of Equation (32) which, as emphasized above, depends also on  $\theta, c, x, y$ . The first element of  $DF_0$  requires computing  $\alpha'(c)$ , which we have already seen. The rest of the elements of  $DF_0$  can be computed by integrating the full unperturbed system (5) together with its variational equations.

When evaluated at the manifold  $\mathcal{K}_0$ , the eigenvectors of  $DF_0$  provide proper directions to split the normal space in stable and unstable directions and hence to obtain the matrix  $N_0(\theta, c)$ .

As shown in Lemma (1), at each point of the manifold  $\tilde{K}_0$  (similarly for  $\mathcal{K}_0$ ) the normal bundle is split in two stable directions and an unstable one. One stable direction is given by the contraction in  $w$ ; the other two are given by the stable and unstable directions of the saddle point  $Q_0$  of system  $\mathcal{X}$ . These directions are given by the eigenvectors of matrix  $DF_0(\tilde{K}_0)$

$$\begin{aligned} v_1^s &= (0, 0, 1, -1/\sqrt{2}, P_{5,3}) \\ v_2^s &= (0, 0, 0, 0, 1) \\ v^u &= (0, 0, 1, 1/\sqrt{2}, P_{5,5}), \end{aligned}$$

with

$$\begin{aligned} P_{5,3} &= \frac{1/\sqrt{2}\partial_y w' - \partial_x w'}{\partial_w w' + 1/\sqrt{2}} \\ P_{5,5} &= -\frac{1/\sqrt{2}\partial_y w' + \partial_x w'}{\partial_w w' - 1/\sqrt{2}}. \end{aligned}$$

Hence,  $N_0(\theta, c)$  becomes

$$N_0(\theta, c) = \begin{pmatrix} 0 & 0 & 0 \\ 0 & 0 & 0 \\ 1 & 0 & 1 \\ -1/\sqrt{2} & 0 & 1/\sqrt{2} \\ P_{5,3} & 1 & P_{5,5} \end{pmatrix}.$$

## 4 Numerical results

We apply the method described in [18], Chapter 5, and summarized in Sections 3.1-3.2. We fix the following parameter values

$$\begin{aligned} G(t) &= \sin(\omega t) & \omega &= 2.1 \\ \lambda &= 0.02 & \tilde{\kappa} &= 1 \end{aligned}$$

and consider different situation regarding parameters  $\varepsilon$ ,  $\tilde{\zeta}$  and  $\tilde{\chi}$ .

In all cases, we use as seed for the Newton method the unperturbed setting shown in Section 3.2 and use cubic spline interpolations in a grid of points

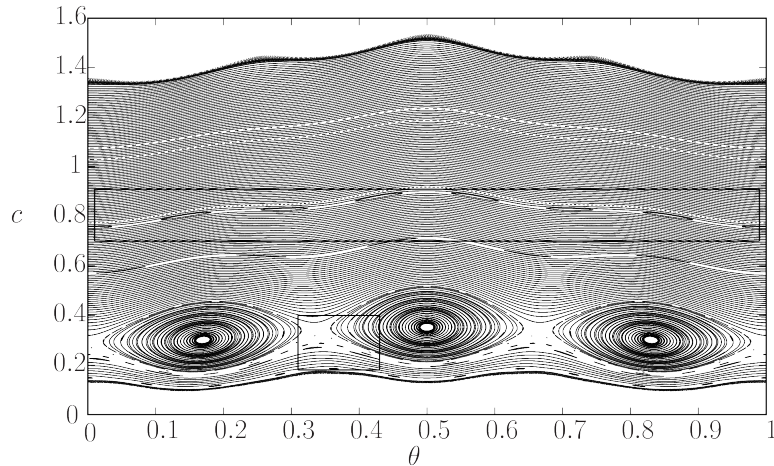


Figure 4: Inner dynamics in  $\tilde{\mathcal{K}}_\varepsilon$  for the conservative case with  $\varepsilon = 6 \cdot 10^{-2}$  and  $\tilde{\zeta} = \tilde{\chi} = 0$ , obtained by iterating the numerically obtained map  $f_\varepsilon(\theta, c)$ . The labeled rectangles are magnified in Figures 7 and 8.

for  $(\theta, c) \in \mathbb{T} \times [0.1, 0.5]$ . At each Newton step, the two substeps explained in Sections 3.1.1 and 3.1.2 are performed for each point of the grid, which allows a natural parallelization. This is done using “open mp” libraries and, ran in a 16 processors node, each Newton step takes around 2 minutes for a grid of  $500 \times 200$  points. The code is available at

[https://github.com/a-granados/nhim\\_parameterization](https://github.com/a-granados/nhim_parameterization)

#### 4.1 Conservative case

We start by setting  $\tilde{\zeta} = \tilde{\chi} = 0$  and  $\varepsilon = 6 \cdot 10^{-2}$ . In this case, as mentioned above, the dynamics of the system restricted to  $\tilde{\mathcal{K}}_\varepsilon$  becomes Hamiltonian. Moreover, for  $\tilde{\zeta} = \tilde{\chi} = 0$  systems  $\mathcal{X}$ ,  $\mathcal{U}$  and  $w$  remain uncoupled. The inner dynamics is given by the one and a half degrees of freedom Hamiltonian system, and therefore  $f_\varepsilon$  becomes a symplectic map. In Figure 4 we show a global illustration of the inner dynamics, where one can see typical objects of this type of maps. The space is mostly covered by KAM invariant curves acting as energy bounds. For the chosen value of  $\omega$  one observes three main resonances:  $3 : 1$ ,  $5 : 2$  and  $7 : 3$ , where  $m : n$  means  $mT = n\alpha(c)$ . These resonances are labeled in Figure 5, where we show the periods of the unperturbed system as a function of  $c$  ( $\alpha(c)$ ), and they approximately correspond

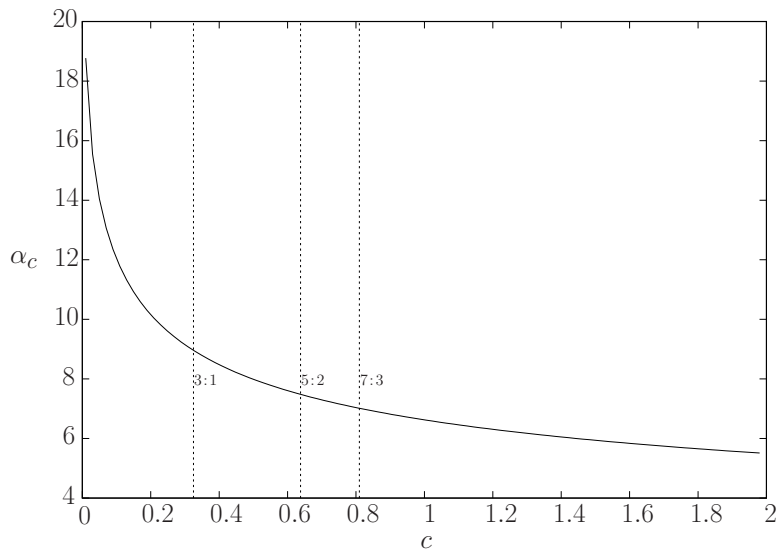


Figure 5: Periods of the unperturbed system,  $\alpha(c)$ .

to the unperturbed periodic orbits  $\mathcal{P}_{0.325}$ ,  $\mathcal{P}_{0.638}$  and  $\mathcal{P}_{0.81}$  defined in Equation (8), respectively. As it comes from Melnikov theory for subharmonics orbits (see [17]), when they persist, one finds an even number of periodic orbits of the stroboscopic map; half are of the saddle and the rest are elliptic; this number is given by the number of simple zeros of the so-called Melnikov function for subharmonic periodic orbits. Recalling that we are dealing with the conservative case ( $\varepsilon > 0$ ,  $\tilde{\zeta} = \tilde{\chi} = 0$ ), in our case this function becomes

$$M(t_0) = \int_0^{mT} vG(t + t_0)dt, \quad (35)$$

where  $v = \Pi_v(\varphi_{\mathcal{U}}(t; 0, \sqrt{2c}))$  is evaluated along the unperturbed periodic orbit,  $\mathcal{P}_c$ , with initial condition at  $u = 0$  such that  $\alpha(c) = mT/n$ . In Figure 6 we show such function for these three resonances. Each of them possesses two simple zeros and, hence, there exist (for  $\varepsilon > 0$  small enough) two periodic points of the stroboscopic map of the saddle and elliptic type. Note that all of them have simple zeros at  $t_0 = 0$ , which, recalling that the initial condition to compute  $M(t_0)$  is taken at  $u = 0$ , implies that the corresponding periodic orbits possess one point  $\varepsilon$ -close to  $\theta = 0$ . Note also that the  $7 : 3$  and  $5 : 2$  Melnikov functions have been magnified by a factor 100 and 10000, respectively, which tells us which of them will first bifurcate when increasing  $\varepsilon$ .

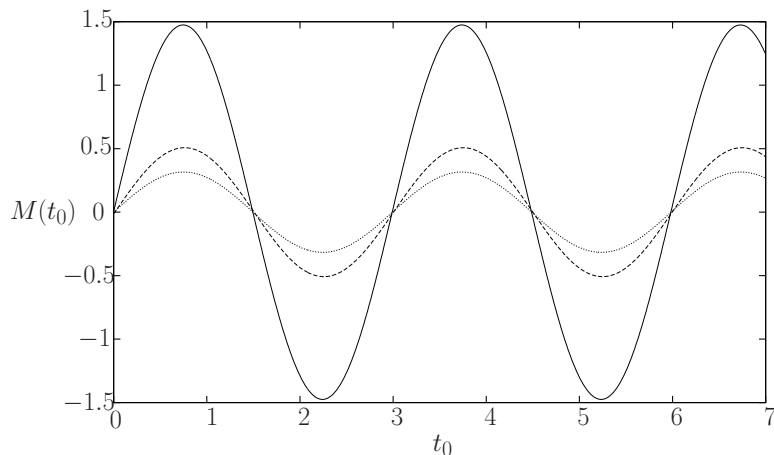


Figure 6: Melnikov functions for the resonances 3 : 1 (solid), 7 : 3 (dashed, magnified by a factor of 100) and 5 : 2 (pointed, magnified by a factor of 10000).

The 3 : 1 periodic orbits are clearly observed in Figure 4. The saddle type one is magnified in Figure 7, where one also observes secondary tori and evidence of chaos given by the homoclinic tangles. The resonance 7 : 3 is magnified in Figure 8.

In Figure 9 we show the inner dynamics in the ambient space. In Figure 9(a) we show the variable  $w$  parameterized by  $\theta$  and  $c$ . Note that it performs oscillations of increasing amplitude with  $c$ . These oscillations can be periodic or quasi-periodic depending on the dynamics of  $\theta$ - $c$ . In Figure 9(b) we see the behaviour of  $x$  and  $y$ . Note that, as system  $\mathcal{X}$  remains uncoupled from the rest of the system and is just periodically perturbed, the hyperbolic equilibrium point  $Q_0$  becomes a  $T$ -periodic orbit and hence a fixed point of the time- $T$  return time. Therefore, in the mentioned figure one observes only a vertical line.

As explained in Section 3, the Newton-like method reported in [18] also provides corrected versions of the normal bundle  $N(\tilde{\mathcal{K}}_\varepsilon)$  (the matrix  $N_\varepsilon$ ); that is, linear approximations of the parameterizations  $W_\varepsilon^{s,\pm}$  and  $W_\varepsilon^{u,\pm}$  given in Equations (24)-(25). In Figure 10 we show the  $x - y - c$  projection of such approximations obtained by slightly varying, for each point at  $\tilde{\mathcal{K}}_\varepsilon$ , the two degrees of freedom of the stable leaf and one degree of freedom of the unstable one. Note that, hence, the stable bundle forms a volume, while the unstable one a tube. In Figures 11 and 12 we show the first 10 iterations

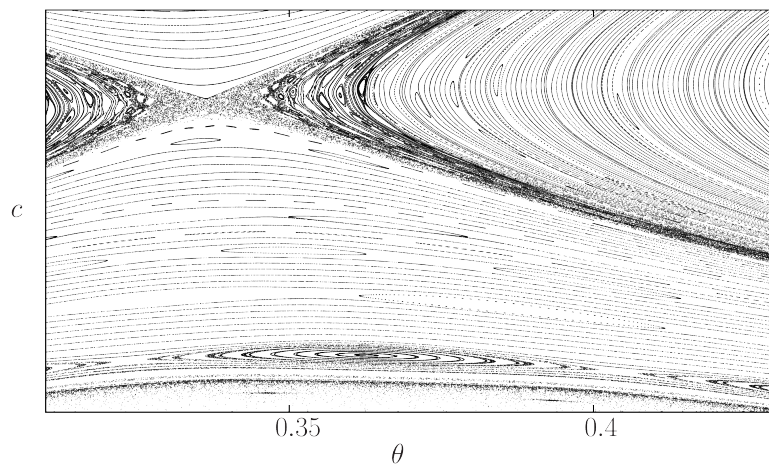


Figure 7: Blow up of the 3 : 1 resonance labeled in Figure 4

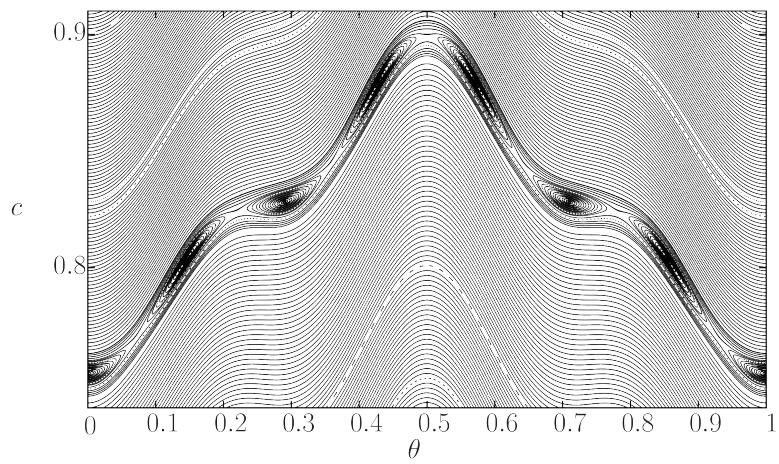


Figure 8: Blow up of the 7 : 3 resonance labeled in Figure 4

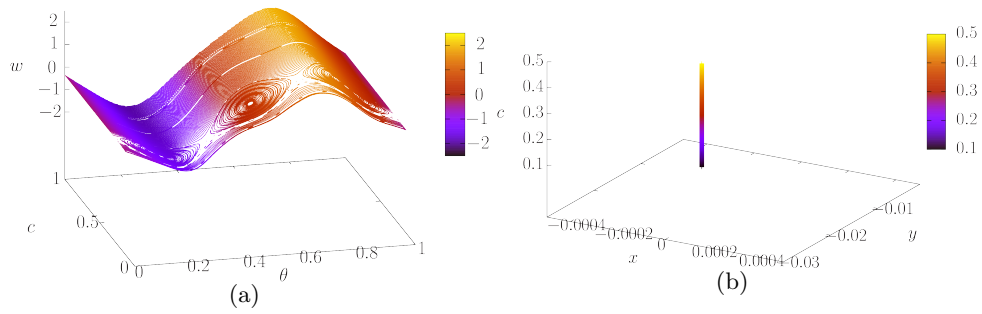


Figure 9: Dynamics restricted to the Normally Hyperbolic Manifold  $\tilde{\mathcal{K}}_\varepsilon$  in the ambient space for the conservative case.

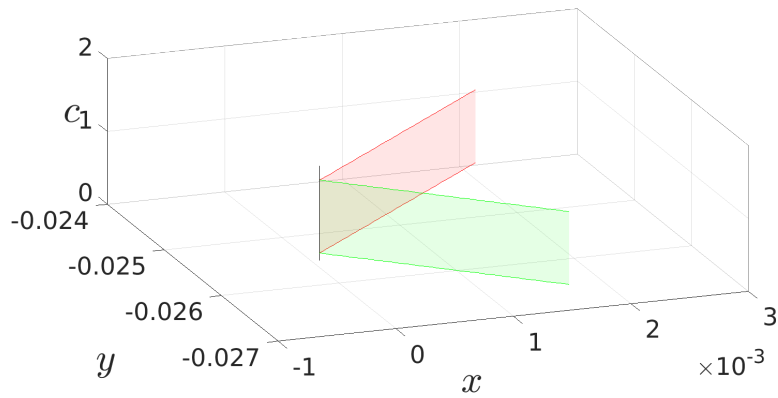


Figure 10: Normal bundle  $N(\tilde{\mathcal{K}}_\varepsilon)$  for the conservative case: tangent space to the stable (green) and unstable (blue) manifolds for  $\varepsilon = 6 \cdot 10^{-2}$  and  $\tilde{\zeta} = \tilde{\chi} = 0$ .

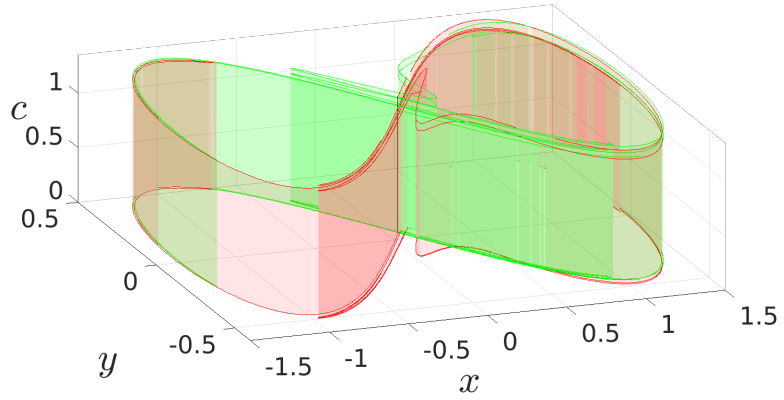


Figure 11: First 10 iterations of the normal bundle shown in Figure 10. Parameter values are  $\varepsilon = 6 \cdot 10^{-1}$  and  $\tilde{\zeta} = \tilde{\chi} = 0$ .

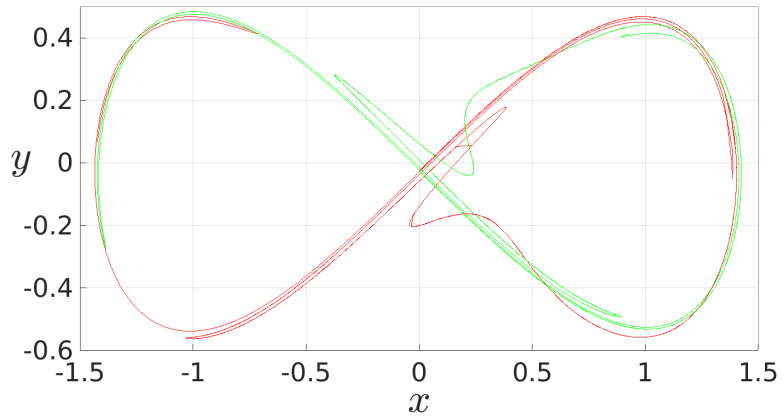


Figure 12: Projection in the  $x - y$  plane of Figure 11.

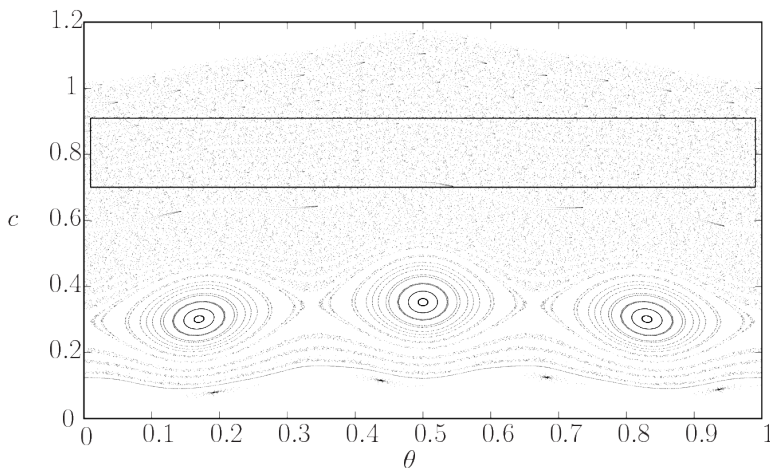


Figure 13: Inner dynamics in  $\tilde{\mathcal{K}}_\varepsilon$  for weak damping:  $\varepsilon = 6 \cdot 10^{-2}$ ,  $\tilde{\zeta} = 6 \cdot 10^{-5}$  and  $\tilde{\chi} = 0$ . We have taken 50 initial conditions at  $\theta = 0.5$  and iterated them 1000 times. The region labeled is maximized in Figure 14, where 400000 iterations are used.

of the stable and unstable normal bundles by  $f_\varepsilon^{-1}$  and  $f_\varepsilon$ , respectively. Figure 11 shows evidence of homoclinic intersections. As the two beams remain uncoupled for  $\tilde{\chi} = 0$ , and the system is conservative, the energy,  $c$ , of system  $\mathcal{U}$  can only vary through the inner dynamics. Hence, such homoclinic excursions do not inject extra energy to the beam represented by system  $\mathcal{U}$ . In other words, the scattering map (see [7, 8]) becomes the identity up to first order terms and there is no hope to observe Arnold diffusion in this case.

## 4.2 Dissipative case

### 4.2.1 Weak damping

When adding small dissipation, hyperbolicity of the saddle periodic orbits guarantees their persistence for small enough dissipation. However, as shown in [24], when perturbed with dissipation, elliptic periodic orbits of area preserving maps become attracting foci. As shown in Figure 13, this occurs with  $f_\varepsilon$  as well. There, 50 initial conditions are taken at  $\theta = 0.5$  and iterated only 1000 times for  $\varepsilon = 6 \cdot 10^{-2}$ ,  $\tilde{\chi} = 0$  and  $\tilde{\zeta} = 6 \cdot 10^{-5}$ , which corresponds to an absolute magnitude of the damping coefficient of  $\varepsilon\tilde{\zeta} = 3.6 \cdot 10^{-6}$ . Some of them are attracted to the 3 : 1 resonant focus, while others skip the

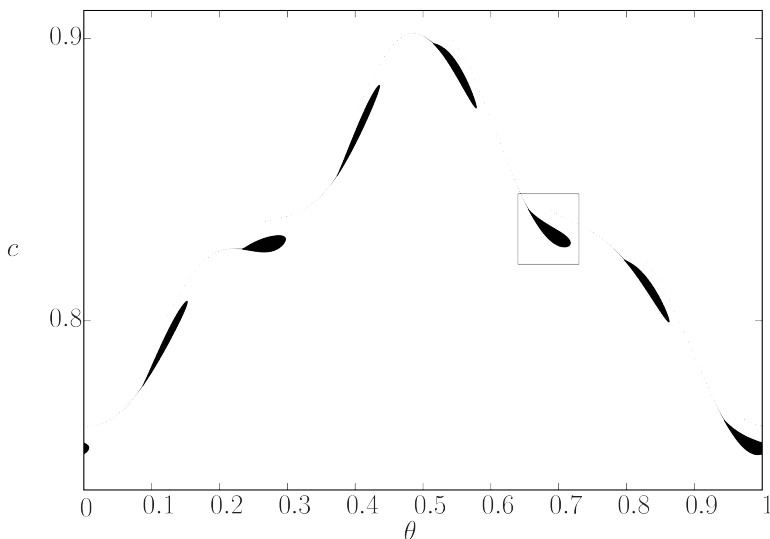


Figure 14: Approximated unstable manifold of the saddle periodic orbits corresponding to 7 : 3 resonance under the presence of small damping:  $\tilde{\chi} = 0$ ,  $\tilde{\zeta} = 6 \cdot 10^{-5}$  and  $\varepsilon = 6 \cdot 10^{-2}$ . The unstable manifold leaves the saddle point and rolls about the 7 : 3 resonant attracting focus. The labeled region is magnified in Figure 15.

separatrices of the saddle 3 : 1 periodic orbit and are attracted to lower energy attractors. In Figures 14 and 15 we show this in more detail for the 7 : 3 resonant periodic orbits. There we have taken an initial condition very close to the unstable manifold of the saddle 7 : 3 resonant periodic orbit. For forwards iterates we see how this unstable manifold slowly rolls about the attracting focus while backwards iterates approach the saddle periodic orbit and rapidly scape due to limited numerical accuracy. This is better appreciated in Figures 16 and 17, where we show the “time” evolution of  $\theta$  and  $c$ , both forwards and backwards in time.

As in the conservative case, due to the lack of coupling between the two beams, the manifold  $\tilde{\mathcal{K}}_\varepsilon$  in the ambient space also looks like a vertical line, similar to Figure 9. Also, the normal bundles and its iterations by  $F_\varepsilon$  and  $F_\varepsilon^{-1}$  look very similar to the ones shown in Figures 10, 11 and 12. Due to these similitudes and taking into account that the coupled case studied in Section 4.2.2 will also add dissipation, we do not show the equivalent results for the case of small damping only.

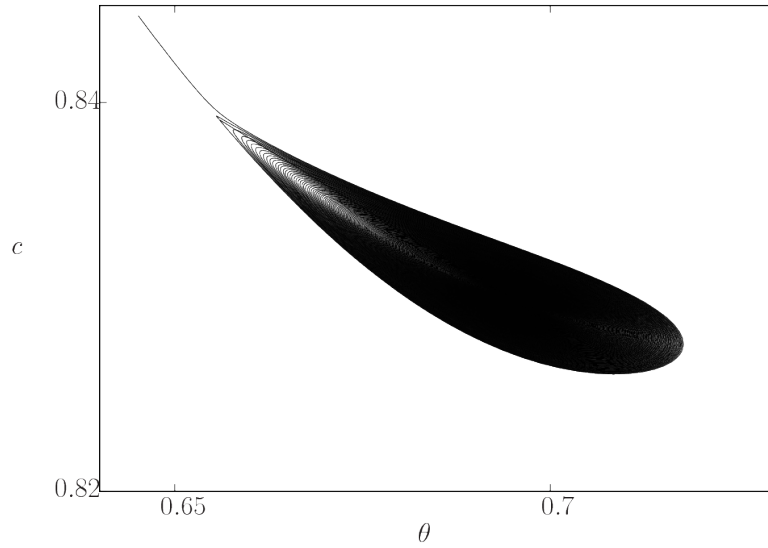


Figure 15: Blow up of the labeled region in Figure 14: unstable manifold of the 7 : 3 resonant periodic orbit under weak damping.

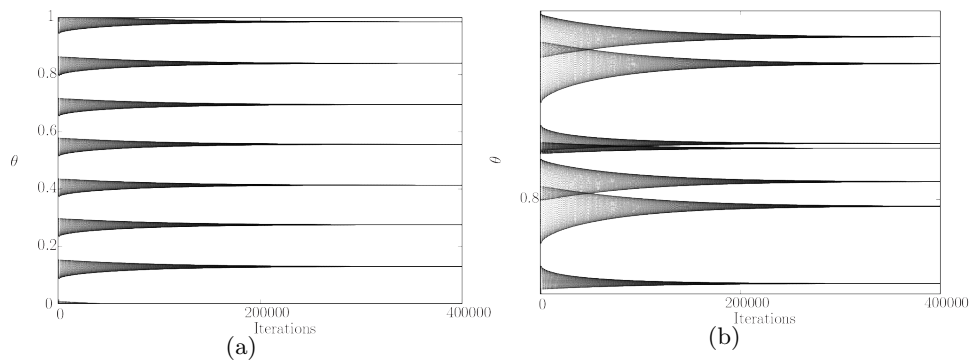


Figure 16: Iterates of  $f_\epsilon$  for the initial condition taken at the unstable manifold shown in Figure 14 and 15.

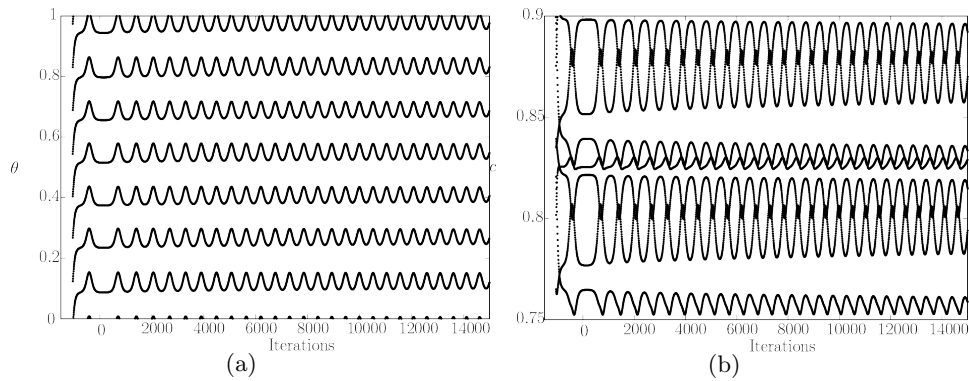


Figure 17: First iterates of  $f_\varepsilon$  and  $f_\varepsilon^{-1}$  for the initial condition taken at the unstable manifold shown in Figures 14 and 15.

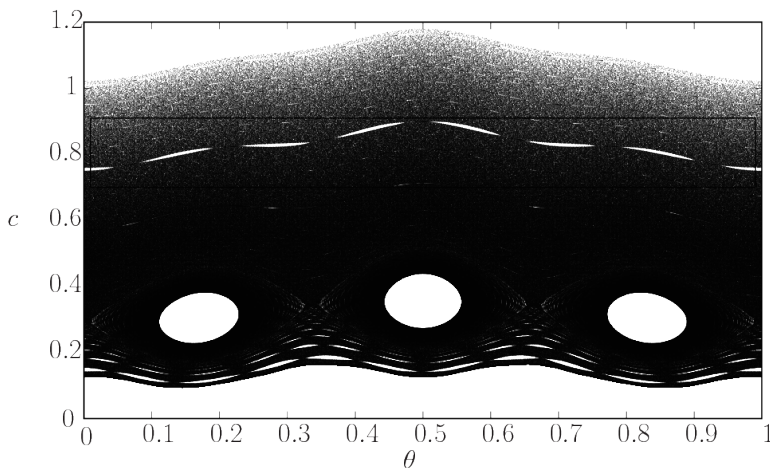


Figure 18: Inner dynamics in  $\tilde{\mathcal{K}}_\varepsilon$  for weak dissipative coupling:  $\varepsilon = 6 \cdot 10^{-2}$ ,  $\tilde{\zeta} = 0$  and  $\tilde{\chi} = 10^{-4}$ .

#### 4.2.2 Weak dissipative coupling

We now study the effect of activating a small dissipative coupling between systems  $\mathcal{X}$  and  $\mathcal{U}$ :  $\varepsilon, \tilde{\chi} > 0$  and  $\tilde{\zeta} = 0$ .

Regarding the inner dynamics, computations reveal that, as one would expect, the effect is similar to the situation given in Section 4.2.1 when only damping on the oscillators was considered. However, by contrast to the previous case, resonant periodic orbits persist for higher values of the dissipative parameter, in this case  $\tilde{\chi}$ .

In Figures 18 and 19 one can see that many of the resonances survive for  $\tilde{\chi} = 10^{-4}$ . As in the only-damping case ( $\varepsilon, \tilde{\zeta} > 0$  and  $\tilde{\chi} = 0$ ), saddle periodic orbits persist while the elliptic ones become attracting foci. In Figure 20 we show the iterates of a point attracted by the 3 : 1 resonant focus. Backwards iterates are also shown until the trajectory scapes.

As shown in Figure 21, for larger values of  $\tilde{\chi}$ , periodic orbits bifurcate and most initial conditions are attracted towards a low energy attractor. For  $\tilde{\chi} = 2 \cdot 10^{-1}$ , the 3 : 1 resonant periodic attracting focus still exists.

In Figure 22 we show the dynamics of  $F_\varepsilon$  restricted to  $\mathcal{K}_\varepsilon$  in the ambient space. In the presence of coupling, the dynamics in the  $x - y$  coordinates are not given by a fixed points anymore. In contrast to the conservative and damped cases studied in Sections 4.1 and 4.2.1, respectively, when  $\tilde{\chi} > 0$  the map  $F_\varepsilon$  restricted to  $\mathcal{K}_\varepsilon$  exhibits oscillations in the  $x - y$  plane of amplitude

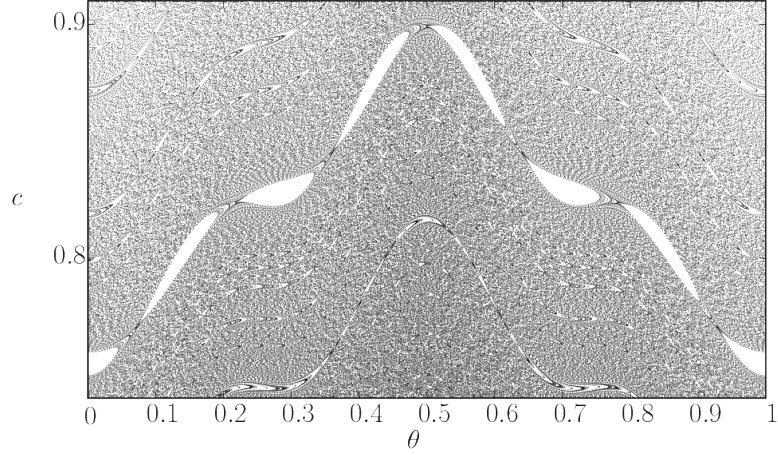


Figure 19: Inner dynamics of the coupled system without damping:  $\varepsilon = 6 \cdot 10^{-2}$ ,  $\tilde{\zeta} = 0$  and  $\tilde{\chi} = 10^{-4}$ . Blow up of the region labeled in Figure 18: inner dynamics around the 7:3 resonant attracting focus.

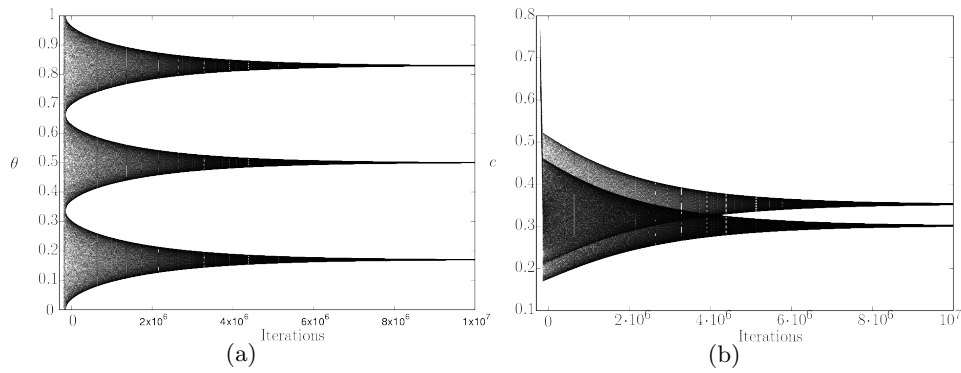


Figure 20: Iterates by  $f_\varepsilon$  and  $f_\varepsilon^{-1}$  of an initial condition attracted by the 3-periodic focus.

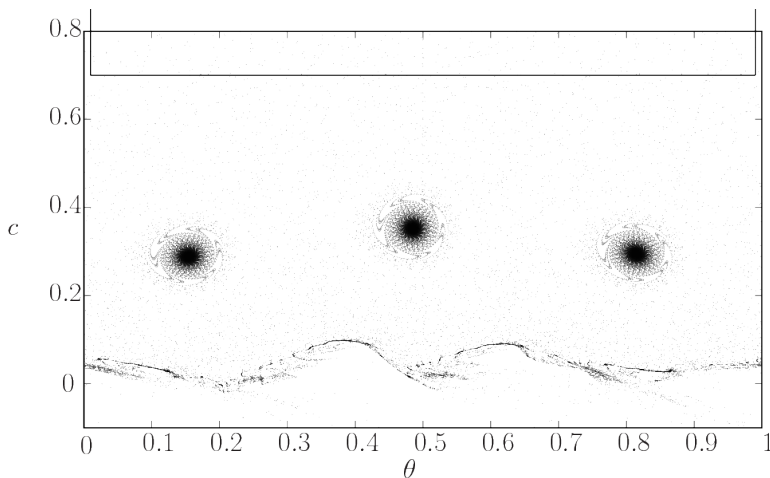


Figure 21: Inner dynamics for  $\varepsilon = 6 \cdot 10^{-2}$ ,  $\tilde{\zeta} = 0$  and  $\tilde{\chi} = 2 \cdot 10^{-1}$ .

$\varepsilon \tilde{\chi}$ .

In Figure 23 we show the  $x - y - c$  projection of the normal bundle  $N(\mathcal{K}_\varepsilon)$  at  $\theta = 0.5$  and  $c \in [0.2, 1]$ . Note that these are the tangent spaces to the stable and unstable manifolds  $W^s(\mathcal{K}_\varepsilon)$  and  $W^u(\mathcal{K}_\varepsilon)$  and hence are good local approximation of those manifolds. When iterated by the global maps  $F_\varepsilon$  and  $F_\varepsilon^{-1}$ , we obtain good approximation of the global unstable and stable manifolds  $W^u(\mathcal{K}_\varepsilon)$  and  $W^s(\mathcal{K}_\varepsilon)$ , respectively. These results are shown in Figures 24 and 25. An animated version of Figure 24 can be found in

<http://agranados.no-ip.org/>

As one can see in Figure 25, there is evidence of the homoclinic intersections as well, which are generically persistent to perturbations due to their transversality. Due to the coupling between the beams, in this case homoclinic excursions may inject extra energy to system  $\mathcal{U}$  and lead to an increase the energy  $c$ . That is, the scattering map may not have vanishing first order terms in  $\varepsilon$ . However, Arnold diffusion is unlikely to exist as the energy gained through homoclinic excursions may not be enough to compensate the loss of energy in the inner dynamics given by the dissipative nature of the coupling.

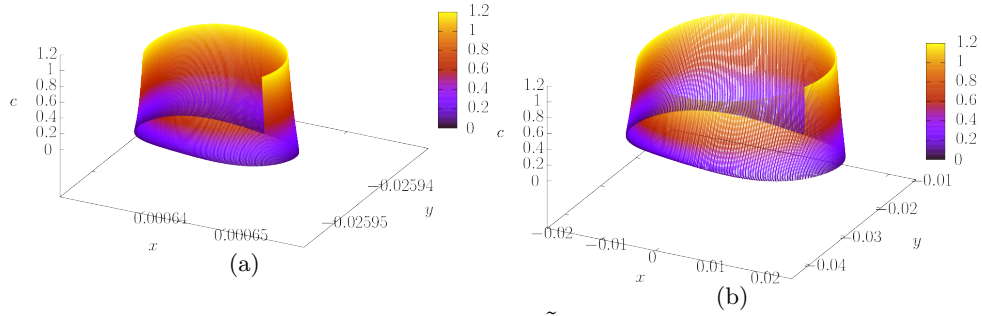


Figure 22: Normally Hyperbolic Manifold  $\tilde{\mathcal{K}}_\varepsilon$  in the ambient space. Parameter values are as in Figure 18 (a) and Figure 21 (b).

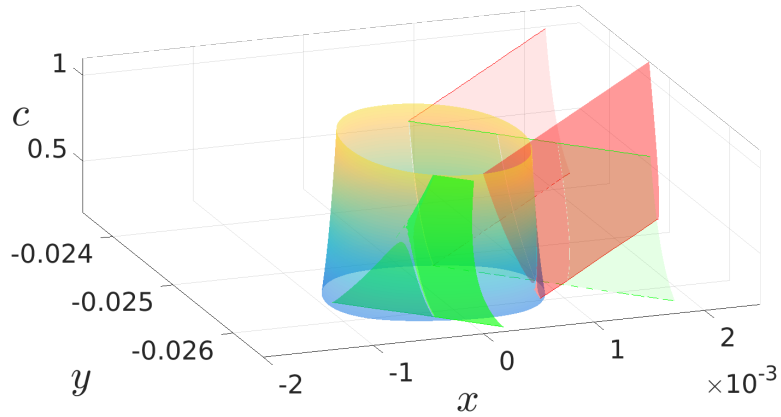


Figure 23: Normally Hyperbolic Manifold  $\tilde{\mathcal{K}}_\varepsilon$  in the ambient space and its Normal bundle  $N(\tilde{\mathcal{K}}_\varepsilon)$  at  $\theta = 0.5$  and  $c \in [0.2, 1]$  Parameter values were for  $\varepsilon = 6 \cdot 10^{-2}$ ,  $\tilde{\zeta} = 0$  and  $\tilde{\chi} = 10^{-2}$ . In light green the tangent space to the stable manifold and its iteration by  $F_\varepsilon^{-1}$  (dark green). In light red the tangent space to the unstable manifold and its iteration by  $F_\varepsilon$  (dark red).

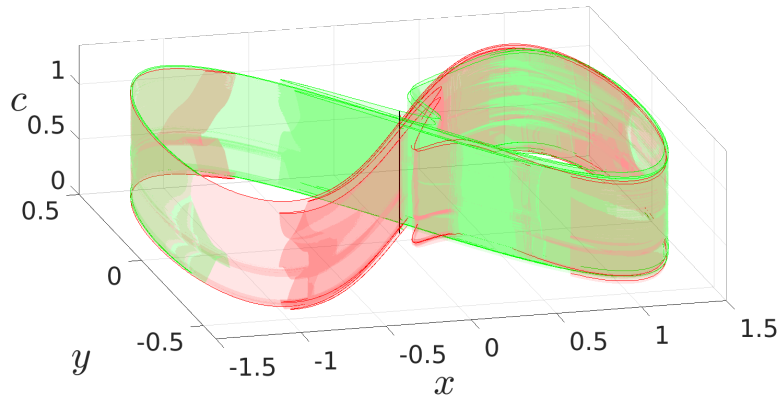


Figure 24: First 10 iterations of the stable and unstable normal bundles shown in Figure 23 by  $F_\varepsilon^{-1}$  and  $F_\varepsilon$ , respectively. In black the manifold  $\tilde{\mathcal{K}}_\varepsilon$ .

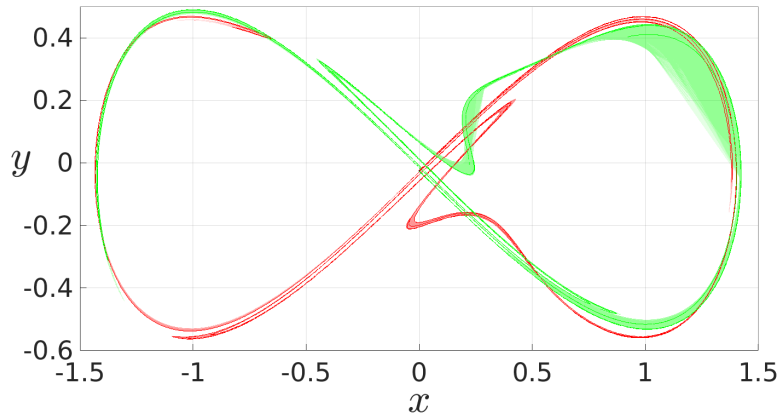


Figure 25: Projection to the  $x - y$  plane of Figure 24

## 5 Conclusions

This paper is a first step towards the use of theory related to Arnold diffusion in energy harvesting systems based on bi-stable oscillators, such as piezoelectric beams or cantilevers. Such theory could be extremely useful in this field, as it precisely deals with the accumulation of energy in oscillators absorbed from a given periodic source.

The dynamics of such systems is given by the coupling of periodically forced Duffing oscillators. The coupling is given by an extra variable (a voltage) which at the same time adds extra dissipation to the intrinsic damping. Moreover, this coupling adds an extra dimension to the system.

In the absence of forcing, damping and coupling, we have proven the existence of a 3-dimensional Normally Hyperbolic Manifold which is “almost” invariant and possesses with 5 and 6-dimensional unstable and stable manifolds. The unperturbed manifold possesses boundaries; despite the system’s dissipation, it persists and is unique. However, the inner dynamics becomes unbounded and hence the manifold needs to be non-uniquely extended beyond the original boundaries.

By implementing the Parameterization method we have computed this manifold, its inner dynamics and good approximations of its stable and unstable manifolds. We have numerically investigated three different situations.

In the absence of damping and coupling, the inner dynamics is given by a symplectic map. Although the stable and unstable manifolds intersect, outer excursions through homoclinic intersections do not inject enough energy to permit the inner dynamics diffuse, because the two oscillators remain uncoupled.

Something similar occurs when the damping is enabled although, in this case, the inner dynamics is not given by an area preserving map. Instead, the inner dynamics at the manifold possesses global attractors.

When the coupling is enabled, we have shown evidence of existence of transversal homoclinic intersections. In this case, although the system may not exhibit diffusion due to the existence of dissipation, outer excursions through homoclinic connections may inject extra energy to overcome the dissipation of inner dynamics. This is extremely desired from the applied point of view and may help to optimize energy harvesting systems based on this type of oscillators.

Future work will include the computation of homoclinic intersection and the scattering map, which is a key tool to quantify the amount of absorbed energy from the source.

## References

- [1] V. I. Arnol'd. Instability of dynamical systems with several degrees of freedom. *Sov. Math. Doklady*, 5:581–585, 1964.
- [2] P. Bernard, V. Kaloshin, and K. Zhang. Arnol'd diffusion in arbitrary degrees of freedom and 3-dimensional normally hyperbolic invariant cylinders. *Acta Mathematica*, 2016. To appear.
- [3] X. Cabré, E. Fontich, and R. de la Llave. The parameterization method for invariant manifolds I: Manifolds associated to non-resonant subspaces. *Indiana Univ. Math. J.*, 52:283–328, 2003.
- [4] X. Cabré, E. Fontich, and R. de la Llave. The parameterization method for invariant manifolds II: Regularity with respect to parameters. *Indiana Univ. Math. J.*, 52:329–360, 2003.
- [5] X. Cabré, E. Fontich, and R. de la Llave. The parameterization method for invariant manifolds III: overview and applications. *J. Diff. Eqts.*, 218:444–515, 2005.
- [6] R. de la Llave. A tutorial on KAM theory. [http://www.ma.utexas.edu/mp\\_arc-bin/mpa?yn=01-29](http://www.ma.utexas.edu/mp_arc-bin/mpa?yn=01-29), 2000.
- [7] A. Delshams, R. de la Llave, and T.M. Seara. A geometric mechanism for diffusion in hamiltonian systems overcoming the large gap problem: Heuristics and rigorous verification on a model. *Memoirs of the American Mathematical Society*, 179, 2006.
- [8] A. Delshams, R. de la Llave, and T.M. Seara. Geometric properties of the scattering map of a normally hyperbolic invariant manifold. *Adv. in Math.*, 217(3):1096–1153, Febraury 2008.
- [9] A. Ertuk, J. Hoffman, and D.J. Inman. A piezomagnetoelastic structure for broadband vibration energy harvesting. *Applied Physics Letters*, 94, 2009.
- [10] A. Erturk and D.J. Inman. An experimentally validated bimorph cantilever model for piezoelectric energy harvesting from base excitations. *Smart Mater. Struct.*, 19, 2009.
- [11] A. Erturk, J.M. Renno, and D.J. Inman. Modeling of Piezoelectric Energy Harvesting from an L-saped Beam-mass Structure with an Application to UAVs. *Journ. Intell. Mat. Sys. Struc.*, 20, 2009.

- [12] J. Fejoz, M. Guardia, V. Kaloshin, and P. Roldan. Kirkwood gaps and diffusion along mean motion resonances in the restricted planar three-body problem. *Jour. Europ. Math. Soc.*, 2016. To appear.
- [13] N. Fenichel. Persistence and smoothness of invariant manifolds for flows. *Indiana Univ. Math. J.*, 21:193–226, 1971/1972.
- [14] M. Ferrari, V. Ferrari, M. Guizzetti, B. Andó, S. Baglio, and C. Trigona. Improved energy harvesting from wideband vibrations by nonlinear piezoelectric converters. *Procedia Chemistry*, 1(1):1203–1206, 2009.
- [15] M. Gidea, R. de la Llave, and T.M. Seara. A General Mechanism of Diffusion in Hamiltonian Systems: Qualitative Results. Preprint available at <http://arxiv.org/abs/1405.0866>, 2014.
- [16] A. Granados, S.J. Hogan, and T.M. Seara. The scattering map in two coupled piecewise-smooth systems, with numerical application to rocking blocks. *Physica D*, 269:1–20, 2014.
- [17] J. Guckenheimer and P. J. Holmes. *Nonlinear Oscillations, Dynamical Systems and Bifurcations of Vector Fields*. Appl. Math. Sci. Springer, 4th edition, 1983.
- [18] Àlex Haro, Marta Canadell, Josep-Lluís Figueras, Alejandro Luque, and Josep-Maria Mondelo. *The Parameterization Method for Invariant Manifolds: From Rigorous Results to Effective Computations*. Springer, 2016.
- [19] I.-H. Kim, H.J. Jung, B.M. Lee, and S.J. Jang. Broadband energy-harvesting using a two degree-of-freedom vibrating body. *Appl. Phys. Lett.*, 98, 2011.
- [20] G. Litak, M.I. Friswell, C.A. Kitio Kwuimy, S. Adhikari, and M. Borowiec. Energy harvesting by two magnetopiezoelastic oscillators. Proceedings of the XI conference on Dynamical Systems, Theory and Applications, Łódź December 2011, 2011.
- [21] A. Luque and D. Peralta-Salas. Arnold diffusion of charged particles in ABC magnetic fields. Preprint available at <http://arxiv.org/abs/1509.04141>, 2015.
- [22] J.-P. Marco. Arnold diffusion for cusp-generic nearly integrable systems on  $\mathbb{A}^3$ . Preprint available at <http://arxiv.org/abs/1602.02403>, 2014.

- [23] F.C Moon and P.J. Holmes. A magnetoelastic strange attractor. *Journal of Sound and Vibration*, 65:275–296, 1979.
- [24] C. Simó and A. Vieiro. Planar radial weakly dissipative diffeomorphisms. *Chaos*, 20, 2010.
- [25] S.C. Stanton, B.A.M. Owens, and B.P. Mann. Harmonic balance analysis of the bistable piezoelectric inertial generator. *Journ. Sound Vibr.*, 331:3617–3627, 2012.
- [26] H. Vocca, I. Neri, F. Travasso, and L. Gammaitoni. Kinetic energy harvesting with bistable oscillators. *Applied Energy*, 97:771–776, 2012.